

REPORT TITLE: Interpretation of Seismic-Reflection Data, Point  
Buchon to San Simeon Point

SIGNATORIES

PREPARED BY: Jan D. Rietman DATE: Sept. 2, 2014

Jan D. Rietman Consulting Geophysicist  
Printed Name Organization

PREPARED BY: H. Gary Greene DATE: Sept. 2, 2014

H. Gary Greene Consulting Geologist  
Printed Name Organization

VERIFIED BY: Stephan A. Graham DATE: 3 Sept. 2014

Stephan A. Graham Consulting Geologist  
Printed Name Organization

APPROVED BY: Richard Klimczak DATE: Sept. 10, 2014

Richard Klimczak Geosciences  
Printed Name Organization

**RECORD OF REVISIONS**

| <b>Rev. No.</b> | <b>Reason for Revision</b>  | <b>Revision Date</b> |
|-----------------|---|----------------------|
| 0               | Initial Report this work is tracked in SAPN 50638227 (Rietman), 505100993 (Greene), and 50533445 (Graham) | 9/2/2014             |
|                 |   |                      |
|                 |   |                      |
|                 |   |                      |
|                 |   |                      |
|                 |   |                      |

## TABLE OF CONTENTS

|   | <b>Page</b> |
|---|-------------|
| Signatories Page .....  | 1           |
| Record of Revisions .....   | 2           |
| Lists of Figures, Plates, and Attachments .....                         | 5           |
| Abbreviations and Acronyms .....  | 7           |
| 1.0 INTRODUCTION .....  | 9           |
| 1.1 Objective .....   | 9           |
| 1.2 Geologic Background .....   | 9           |
| 1.2.1 Regional Stratigraphy .....                                       | 10          |
| 1.2.2 Tectonic Setting .....  | 10          |
| 1.3 Purpose and Scope of This Interpretation .....                      | 10          |
| 1.4 Previous Investigations .....                                       | 11          |
| 2.0 DATABASE .....  | 14          |
| 2.1 Multibeam Echosounder and DEM Data .....                            | 14          |
| 2.2 USGS 2008–2009 High-Resolution 2D LESS and Magnetometer Data .....  | 15          |
| 2.3 PG&E Point Buchon LESS Data .....                                   | 16          |
| 2.4 COMAP Alaska 1986 CDP Survey for PG&E .....                         | 17          |
| 2.5 LTSP 1988 Maps and Legacy Data .....                                | 18          |
| 3.0 TECHNICAL APPROACH .....  | 19          |
| 3.1 Use of IHS Kingdom Program .....                                    | 19          |
| 3.2 Criteria for Data Quality Evaluation .....                          | 21          |
| 3.3 Criteria for Mapping Structural Trends .....                        | 21          |
| 3.4 Accuracy Limitations in Mapping Structural Trends .....             | 22          |
| 4.0 INTERPRETATIONS AND ANALYSES .....                                  | 24          |
| 4.1 The Hosgri Fault Zone .....   | 24          |
| 4.1.1 The HFZ—Point Buchon to Offshore Cambria .....                    | 24          |
| 4.1.2 Fluid-Induced Slope Failures Along the Western HFZ Trend .....    | 27          |
| 4.2 The HFZ Transition to the Piedras Blancas Fault and Fold Belt ..... | 29          |
| 4.3 The Los Osos Fault Zone .....                                       | 30          |
| 4.4 The Half Graben Fault Zone Offshore of Cambria .....                | 31          |
| 4.5 The “Cambria Gap” and the San Simeon Fault Zone .....               | 33          |

|     |   |    |
|-----|---|----|
| 4.6 | Unassigned Fault Zones .....                  | 36 |
| 5.0 | COMPARISON WITH PREVIOUS INTERPRETATIONS..... | 38 |
| 5.1 | The 1988 and 1990 LTSP Maps.....              | 38 |
| 5.2 | Willingham et al. (2013) Paper .....          | 39 |
| 5.3 | Johnson and Watt (2012) Paper.....            | 40 |
| 5.4 | PG&E (2013a) Report .....                     | 40 |
| 6.0 | CONCLUSIONS .....                             | 41 |
| 7.0 | LIMITATIONS .....                             | 44 |
| 8.0 | IMPACT EVALUATION .....                       | 45 |
| 9.0 | REFERENCES .....                              | 46 |

## LISTS OF FIGURES, PLATES, AND ATTACHMENTS

### Figures

- Figure 1.2-1 Study Area Index Map
- Figure 1.2-2 Tectonic Setting
  
- Figure 3.2-1 Record Example—Shallow Bedrock
- Figure 3.2-2 Record Example—Missing Data
- Figure 3.2-3 Record Example—Multiples
- Figure 3.3-1 Record Example—Small-Scale Structures
- Figure 3.3-2 Record Example—Diffractions and Possible Out-of-Plane Reflections
- Figure 3.3-3 Record Example—Low Resolution
  
- Figure 4.1-1 Hosgri Fault Zone—Southern Area
- Figure 4.1-2 Hosgri Fault Zone—Bedrock Outcrop Area
- Figure 4.1-3 Hosgri Fault Zone—Multiple Fault Traces
- Figure 4.1-4 Hosgri Fault Zone—Adjacent Kink Fold
- Figure 4.1-5 Hosgri Fault Zone—No Apparent Fault
- Figure 4.1-6 Hosgri Fault Zone—Northern Area
- Figure 4.1-7 Hosgri Fault— Slope Failure Features
- Figure 4.2-1 Hosgri Fault Zone—Northwest End
- Figure 4.2-2 Structures 6 km North of Hosgri Fault
- Figure 4.2-3 Unassigned Fault Traces North and Parallel to Hosgri Trend, 5 km South of San Simeon Point
- Figure 4.2-4 Shallow Folds and Faults on Southwest Flank of Piedras Blancas Antiform, 4 to 6 km Southwest of San Simeon Point
- Figure 4.2-5 Piedras Blancas Fault and Fold Belt, Southwest Flank of Antiform
- Figure 4.2-6 Piedras Blancas Fault and Fold Belt, Northeast of Figure 4.2-5
- Figure 4.3-1 Los Osos Fault—Southeastern Section
- Figure 4.3-2 Los Osos Fault—Central Section
- Figure 4.3-3 Los Osos Fault—Northern Section
- Figure 4.4-1 Half Graben Fault—South End, LESS Record Example
- Figure 4.4-2 Half Graben Fault—South End, CDP Record Example

- Figure 4.4-3 Half Graben Fault—Central Area
- Figure 4.4-4 Half Graben Fault—South End of Scarp
- Figure 4.4-5 Half Graben Fault—Center of Scarp
- Figure 4.4-6 Half Graben Fault—North End of Scarp
- Figure 4.5-1 San Simeon—Cambria Gap Area—2.5 km North of Half Graben Fault
- Figure 4.5-2 San Simeon—Cambria Gap Area—4 km North of Half Graben Fault
- Figure 4.5-3 San Simeon—Cambria Gap Area—5.5 km North of Half Graben Fault
- Figure 4.5-4 San Simeon—Cambria Gap Area—6.5 km North of Half Graben Fault
- Figure 4.5-5 San Simeon Fault—South End
- Figure 4.5-6 San Simeon Fault—North End
- Figure 4.6-1 Unassigned Faults Offshore of Irish Hills

## **Plates**

- Plate 1 Regional Bathymetry
- Plate 2 Regional Structural Trends and Marine Magnetic Anomalies
- Plate 3 Limited Data Areas
- Plate 4 Southern Area Structural Trends
- Plate 5 Central Area Structural Trends
- Plate 6 Northern Area Structural Trends
- Plate 7 Sediment Thickness Along Half Graben Fault

## **Attachments**

- Attachment 1 Report Verification Summary

## ABBREVIATIONS AND ACRONYMS

|       |  |
|-------|--|
| 2D    | two-dimensional  |
| 3D    | three-dimensional  |
| AB    | Assembly Bill  |
| CDP   | common depth point   |
| CEC   | California Energy Commission   |
| CRADA | Cooperative Research and Development Agreement (between PG&E and the USGS) |
| CSUMB | California State University, Monterey Bay                                  |
| DCPP  | Diablo Canyon Power Plant  |
| DEM   | digital elevation model  |
| DGPS  | differential global positioning system                                     |
| FCL   | Fugro Consultants, Inc.  |
| FSAR  | Final Safety Analysis Report   |
| GPS   | global positioning system  |
| HESS  | high-energy seismic-reflection surveys                                     |
| HFZ   | Hosgri fault zone  |
| Hz    | hertz  |
| IHO   | International Hydrographic Office  |
| IMU   | inertial motion unit   |
| ITR   | Independent Technical Reviewer   |
| J     | joule  |
| kHz   | kilohertz  |
| kJ    | kilojoules   |
| km    | kilometers   |
| LESS  | low-energy seismic-reflection surveys                                      |
| LiDAR | light detection and ranging  |
| LTSP  | Long Term Seismic Program  |
| m     | meters   |
| MBES  | multibeam echosounder  |
| MLLW  | mean-lower-low-water   |
| mm/yr | millimeters per year   |

|        |   |
|--------|---|
| ms     | milliseconds  |
| NAD 27 | North American Datum of 1927                          |
| NGDC   | National Geophysical Data Center                      |
| NOAA   | National Oceanographic and Atmospheric Administration |
| NRC    | Nuclear Regulatory Commission                         |
| PG&E   | Pacific Gas and Electric Company                      |
| QA     | quality assurance                                     |
| QC     | quality control                                       |
| RTK    | real-time kinematic                                   |
| s      | seconds   |
| SSC TI | Seismic Source Characterization Technical Integration |
| SSHAC  | Senior Seismic Hazard Advisory Committee              |
| TWTT   | two-way travel time                                   |
| USGS   | U.S. Geological Survey                                |
| UTM    | Universal Transverse Mercator                         |
| WGS 84 | World Geodetic System of 1984                         |



## **1.0 INTRODUCTION**

This interpretation of seismic-reflection data for the offshore area between Point Buchon and San Simeon Point is part of Pacific Gas and Electric Company's (PG&E) low-energy seismic-reflection survey (LESS) investigations of the relationships between the Hosgri fault zone (HFZ) and other fault zones near the Diablo Canyon Power Plant (DCPP). This work is being done by PG&E to comply with the California Energy Commission's (CEC) recommendation, as reported in the CEC's November 2008 report titled "An Assessment of California's Nuclear Power Plants: AB 1632 Report," that PG&E use three-dimensional (3D) seismic-reflection mapping and other advanced geophysical techniques to explore fault zones near the DCPP.

As part of the effort to understand the seismic hazards within the region of the DCPP, PG&E has collected new 3D and 2D data sets and integrated U.S. Geological Survey (USGS) LESS data sets with higher-power common-depth-point (CDP) seismic-reflection survey data from the Long Term Seismic Program (LTSP; PG&E, 1988). This interpretation uses the USGS LESS data from 2008 and 2009 surveys that were integrated with the CDP data from the COMAP 1986 and Western Geophysical Surveys of 1975 to 1982. The CDP surveys are part of PG&E's legacy archive data.

This interpretation report and associated figures and plates are subject to PG&E Geosciences' Quality Assurance (QA) program, under 10CFR 50 Appendix B, and have been reviewed by a formal Independent Technical Reviewer (ITR). This technical review has been undertaken by Professor Stephan Graham of Stanford University and his comments have been considered in this final draft.

### **1.1 Objective**

The objective of this technical report is to present a geologic interpretation of the existing shallow-penetration (LESS) and older deep-penetration (CDP) seismic-reflection profile data north of the DCPP in the offshore area between Point Buchon and San Simeon Point. This area includes the Hosgri, Los Osos, and San Simeon fault zones, as well as currently unnamed faults in Estero Bay and along the southern flank of the Piedras Blancas Antiform at the north end of the study area. The interpretation of the seismic data is presented as a series of structural trend maps. Other data sets, including multibeam bathymetry, marine magnetometer survey data, and earthquake seismicity data are presented as maps or overlays and integrated into the seismic data interpretation. The final integrated interpretation is intended to be used further in the evaluation of seismic hazards of the region and their potential impact on the DCPP.

### **1.2 Geologic Background**

This section presents a brief summary of the regional stratigraphic and tectonic setting of the study area to provide a contextual framework for the observations and interpretations made from the examined data sets. The study area consists of the offshore area from Point Buchon north to San Simeon Point, including the continental shelf (Figure 1.2-1). The study area overlaps with the northern tip of the PG&E Point Buchon 3D/2D LESS

study (PG&E, 2012) and the northern part of the PG&E seismic stratigraphy study (PG&E, 2013).

### **1.2.1 Regional Stratigraphy**

Generally, the stratigraphy that exists on the Point Buchon to San Simeon Point continental shelf is composed of unconsolidated Quaternary sediments that overlie an erosional top-of-Neogene bedrock surface. Offshore sedimentary bedrock and basement rock identifications in the study area are based on dive observations, bottom samples, and cores presented in the LTSP Report (PG&E, 1988) and Willingham et al. (2013). Bedrock is primarily of sedimentary rocks unconformably resting on basement rocks. Basement rocks exposed in the offshore Central California coastal region generally consist of Jurassic to Cretaceous Franciscan Complex rocks (primarily mélangé, metavolcanics, ophiolite, and serpentine) faulted against Cretaceous marine arkosic to lithic sandstone. Geologic mapping reported in the Shoreline Fault Zone Report (PG&E, 2011a, 2011b) shows that the seafloor is underlain by Quaternary marine sediment for a large part of the study area. Where this sediment is absent, most of the seafloor is underlain by Tertiary strata exposed in stratigraphic sequence from south to north, including Obispo Formation, Monterey Formation, and the Miguelito Member of the Pismo Formation. Pliocene Pismo Formation unconformably overlies the Monterey Formation.

### **1.2.2 Tectonic Setting**

The central coast of California is characterized by transpressional deformation between the San Andreas fault zone to the east and the San Gregorio–San Simeon–Hosgri system of near-coastal faults to the west. Transpressional deformation in the region is likely driven by three distinct but interacting processes (Lettis et al., 2004):

1. Northward left transfer of slip from the San Andreas fault zone to the Reliz-Rinconada and West Huasna faults to the Hosgri–San Simeon fault zones.
2. Clockwise rotation of the western Transverse Ranges domain, which imparts north-directed strain in the region.
3. An unknown amount of possible plate-normal convergence across the region.

Transpressional deformation has produced several distinct but interacting crustal domains and tectonic structures (PG&E, 1988). The study area lies in the northern part of the Los Osos domain, a triangular-shaped structural terrane consisting of northwest-striking reverse, oblique, and strike-slip faults that border uplifted blocks and subsiding basins within the domain (Figure 1.2-2). Details of the structural features in the Los Osos domain are given in PG&E (1988, 2011b, 2013).

## **1.3 Purpose and Scope of This Interpretation**

The area of this study, Point Buchon to San Simeon Point, includes the southern offshore extension of the San Simeon fault zone, the northern termination of the HFZ, intervening structures between the two fault zones, and the offshore extension of the Los Osos fault

zone into Estero Bay. All of these structures contribute to the seismic hazard at the DCP.P and were the subject of previous investigations in the initial Final Safety Analysis Report (FSAR; PG&E, 1974) of the DCP.P and the subsequent LTSP effort (PG&E, 1988, 1990). Since 2009, PG&E has acquired additional seismic-reflection data sets in this area, including new data collected by the USGS (Sliter et al., 2009) and pre-1989 exploration industry data that were proprietary until publically released in 2005. The later data sets are now on file at the USGS and are included in PG&E's geophysical survey legacy data archive.

The purpose of this study is to review and interpret all seismic-reflection data in and around the intersection of the San Simeon fault and the HFZ offshore of Cambria. Specific tasks included project setup, data interpretation, and reporting and documentation, as described briefly below.

- **Project setup** included defining the seismic data sets in the project area and incorporating them into an IHS Kingdom™ software program. Existing maps of previous interpretations of seismic-reflection data from this area were converted to World Geodetic System of 1984 (WGS 84) projection and loaded into the Kingdom program so that comparisons could be made with the new interpretations. Although this project was not originally subject to the QA process applied to the most recent PG&E 3D LESS studies (GEO.DCP.P.TR.14.02), we used a version of the Kingdom program for our interpretations that is one of the 64-bit Version 8.6 copies vetted for nuclear use by PG&E in the recent LESS studies, and thus wrote this technical report under QA..
- **Data interpretation** included developing two picks (one for each author) of independent sets of faults (and other structures) and consolidating them into a single consensus fault map (structural trend map). Supporting interpretational products included mapping of one or more unconformities and an isopach (thickness) map of a sediment unit related to the unconformities.
- **Project reporting and documentation** included preparing this report and associated illustrations (figures and plates) and presenting the results to PG&E. Supporting tasks, including converting previous map projections (North American Datum of 1927 [NAD 27]) to the WGS 84 projections and preparing the plates and figures for the report, were completed by Lettis Consultants International, Inc., under separate contract.

## 1.4 Previous Investigations

The geologic structures of interest in this study lie primarily offshore, and the principal evidence for their locations and physical properties comes from the analysis of marine seismic-reflection data. Petroleum exploration of the study area (part of the offshore Santa Maria Basin) began in the 1960s with regional seismic-reflection profiling, gravity, and magnetic surveys. Hoskins and Griffiths (1971) first published evidence of a major fault offshore of the south-central California coast, and the fault was later defined in more detail based on a USGS seismic-reflection survey that showed that the HFZ exhibited

seafloor expressions. The fault name “Hosgri” is a contraction of the Hoskins and Griffiths’ names (Wagner, 1974).

In the early 1970s, PG&E began construction and licensing processes for the DCP.P. The existence of the HFZ approximately 4 km offshore prompted high-resolution seismic-reflection surveys by the USGS and PG&E to better define the limits, near-surface characteristics, and recency of activity of the fault zone. In 1973 and 1974, PG&E collected over 1,300 km of high-resolution seismic-reflection data, much of it within this study area. However, the deeper penetration exploration lines in this area were still on a regional spacing and many of the lines did not approach the coast closely enough to provide good images of the HFZ. As a result, the character of the fault zone was sufficiently nondescript so that it could be used to encompass a variety of tectonic models, including coastal California fault zones having major lateral displacement. In several tectonic analyses published in the late 1970s, the HFZ was associated with the San Gregorio–Sur–San Simeon fault system that extended northwest from San Simeon Point (Hall, 1975; Hamilton and Willingham, 1977; Graham and Dickinson, 1978; Silver and Normark, 1978). However, none of these papers provided direct evidence of the connection between the HFZ and the San Simeon fault, and other authors interpreted the HFZ as passing west of San Simeon Point to the vicinity of the Piedras Blancas antiform (Hoskins and Griffiths, 1971; Buchanan-Banks et al., 1978).

Leslie (1981) used the 1970s USGS and the 1973 and 1974 PG&E survey data sets to study the northern termination of the HFZ in the nearshore area north of Estero Bay. He interpreted the data to demonstrate a connection between the HFZ and the onshore San Simeon fault. He also interpreted that the associated seafloor features indicated Holocene activity in this area. This interpretation was adopted in maps published by the California Division of Mines and Geology (Kennedy et al., 1987; Greene and Kennedy, 1989; Jennings, 1994) and by McCulloch (1987).

In 1983, PG&E began the LTSP and commissioned a multichannel seismic-reflection survey in California State waters from north of the Piedras Blancas antiform to south of the DCP.P. This 1986 survey (Section 2.4) was one of the last high-energy seismic-reflection surveys (HESS) permitted in California State waters. For the LTSP, PG&E also purchased additional exploration survey lines in this same general area between San Simeon Point and the DCP.P. These lines were primarily from the Western Geophysical surveys of 1974, 1975, and 1982. The interpretation of these new data sets was integrated with the 1970s PG&E data and presented in the LTSP documentation (PG&E, 1988, 1990). These data were interpreted to show several normal faults that formed half-graben-type structures. The normal faults began offshore of Point Estero at the north end of Estero Bay and generally trended toward San Simeon Point. However, direct connections between the several normal faults or with the HFZ or San Simeon fault could not be established with these data sets (PG&E, 1988, 1990). This zone of normal faults between the HFZ and the onshore San Simeon fault was interpreted as a step-over pull-apart basin (DiSilvestro et al., 1990; Lettis et al., 1990). Although the direct connection between the HFZ and the San Simeon fault was not established in the available seismic-reflection data, regional tectonic analysis evaluation of relative offsets of geological

terrane considered the HFZ as part of the San Gregorio–Sur–San Simeon–Hosgri coastal fault zone (Dickinson et al., 2005).

In 2008 and 2009, the USGS conducted single-channel high-resolution surveys in this study area (Sliter et al., 2009; see Section 2.2). Although this was a low-energy survey, it was apparently the first seismic-reflection data collected in the San Simeon–Estero Bay offshore area since the 1989 limitations on seismic survey energy levels in California State waters. Line spacing was originally 800 meters (m), with additional lines providing a 400 m spacing in selected areas. The consequent USGS interpretation of these data was published by Johnson and Watt (2012). They concluded that the data provided evidence that the HFZ offshore of Point Buchon continued to the north, passing through several significant releasing and restraining bends before passing on land at San Simeon.

In 2012, PG&E requested that the authors of this report conduct an independent interpretation of the USGS data and compare the results with the Johnson and Watt (2012) interpretation, as well as interpretations based on other PG&E studies (Hanson et al., 2004; Lettis et al., 2004; Willingham et al., 2013). The interpretation presented in this report is based on the USGS high-resolution seismic-reflection profile data integrated with multibeam echosounder (MBES) bathymetry data displayed as a digital elevation map (DEM) and the higher-energy seismic-reflection data collected in the 1970–1986 period.

## 2.0 DATABASE

The database used for this investigation consists of a variety of geophysical data, as follows:

- Multibeam echosounder (MBES) bathymetry.
- Low-energy shallow-penetration seismic-reflection profiles from the USGS 2008 and 2009 surveys.
- High-energy deep-penetration seismic-reflection profile data from the PG&E geophysical survey legacy data archive.
- 2D seismic-reflection profile data from the 3D LESS study offshore of Point Buchon (PG&E, 2013a).
- LTSP maps and data (PG&E, 1988; Willingham et al., 2013).

Supplementary data provided to PG&E by the USGS include marine magnetometer anomaly maps (Sliter et al., 2009; Johnson and Watt, 2012) and earthquake epicenter locations and depths (Hardebeck, 2014). These data were integrated into the interpretation of the structural geometry of the region.

### 2.1 Multibeam Echosounder and DEM Data

The MBES bathymetry and backscatter data from the San Simeon Point to Estero Bay nearshore region were acquired using a combination of sonar systems (400 kHz Reson 7125, 240 kHz Reson 8101, and SEA SWATHplus) aboard the R/V *Ven Tresca* by the Seafloor Mapping Lab at California State University, Monterey Bay (CSUMB) in 2007, 2009, and 2010. The data extend from approximately 10 m water depth nearshore to the California State waters territorial boundary 3 nautical miles from shore. Data collection standard was maintained at International Hydrographic Office (IHO) S-44 Special Order specifications. Across the entire MBES swath, an average of 95.8 percent of crossline soundings fell within IHO Special Order tolerances, with 99.7 percent within IHO Order 1 (PG&E, 2012) and processed at 2 m grids at an approximate  $\pm 1$  m resolution.

Specifically, the data accuracy ranges from 1 m horizontal resolution for data from 0 to 50 m depth, and 2 m horizontal resolution for data at greater depths. The vertical precision of the data is  $\pm 10$  centimeters (cm; see Appendix F of PG&E, 2011b). Position and altitude during data collection were obtained through an Applanix POS MV 320™ V4 system with TrueHeave™ processing, which accounted for vessel motion such as heave, pitch, and roll (position accuracy  $\pm 2$  m; pitch, roll, and heading accuracy  $\pm 0.02$  degrees; heave accuracy  $\pm 5\%$  or 5 cm), with input from a C-Nav-enabled NavCom 2050™ global positioning system (GPS). Additionally, kinematic GPS altitude data were used to account for tide-cycle fluctuations, and sound-velocity profiles were collected with an Applied Microsystems SV Plus™ sound velocimeter. Hillshade images that were developed from the DEM compiled for PG&E (2013b) contained both onshore light detection and ranging (LiDAR) images and offshore MBES bathymetry data.

Additional MBES data were collected by the USGS in 2012, under support from PG&E, using the R/V *Parke Snavely* and have recently been released for use in this study. Both

MBES bathymetry and co-registered acoustic backscatter data were collected in a 165-square-mile area in water depths ranging from 45 to 250 m using a Reson SeaBat 7111™ sonar (Hartwell et al., 2013). This survey completed MBES coverage within Estero Bay and extends the area covered to beyond the distal edge of the continental break. The data were processed using Caris HIPS and SIPS software and gridded to 2 m bins for data collected in less than a 100 m of water, and 4 m bins for data collected below 100 m depth. Real-time kinematic (RTK) GPS position and inertial measurement data were recorded using an inertial motion unit (IMU) and were surveyed in place to a common reference frame with a Geodimeter 640™ Total Station (Hartwell, 2013).

Geodetic control for the USGS 2012 survey was established using an Applanix POS MV 320™ system with two GPS antennas and two low-noise survey-grade 72-channel receiver cards embedded in the POS computer system, which computes position to 0.02 m with RTK (Hartwell, 2013). Sound-velocity measurements were collected continuously using an Applied Microsystems Micro SV™ deployed on the transducer frame for real-time velocity adjustments at the transducer-water interface. The Micro SV is accurate to  $\pm 0.03$  meter per second, and sound-velocity profiles were collected with an Applied Microsystems, AvPlus 3472™. Specifications and accuracies of the systems used by the USGS can be found in Hartwell et al. (2013).

The regional bathymetry is shown on a map of the study area based on the above-referenced surveys (Plate 1). Water depths in the survey area are referenced to mean-lower-low-water (MLLW) and range from less than  $-10$  m to deeper than  $-300$  m.

The onshore topography and coastal zone images on the plates are from a composite DEM developed by PG&E as part of the DCP.P Geodatabase (PG&E, 2013b). The DEM extends along the Central California coastal area from south of San Luis Obispo Bay to north of San Simeon Point. The DEM is a composite of 116 data layers that were mosaicked using bilinear interpolation to minimize edge effects at the borders of individual data sets. In addition to the MBES surveys discussed above, the following major coastal zone DEM sources are shown on the plates:

- Regional DEM from National Geophysical Data Center (NGDC) Coastal Relief Model, Vol. 06.
- California State Coastal Conservancy Coastal LiDAR Project, the National Oceanographic and Atmospheric Agency (NOAA) Coastal Service Center.
- PG&E LiDAR Surveys:
  - San Simeon and Cambria Faults Survey in 2013
  - San Luis Range and Los Osos–Edna Valleys Survey in 2011
  - DCP.P Coastline Survey in 2010

## **2.2 USGS 2008–2009 High-Resolution 2D LESS and Magnetometer Data**

Single-channel seismic-reflection profile data were acquired in 2008 and 2009 by the USGS between Piedras Blancas and Pismo Beach, along shore-perpendicular transects spaced 800 m apart extending beyond the 3-mile limit of California State waters (Sliter et

al., 2009). Data were collected from the R/V *Parke Snavely* using a SIG 2Mille™ mini-sparker and an EdgeTech SB-0512i™ chirp system. The SIG mini-sparker system used a 500-joule (J) high-voltage electrical discharge and a towed 15 m hydrophone streamer received the resulting acoustic energy. The mini-sparker source was fired at a rate of two times per second (s), which generally gave a data trace every 1 m and record lengths of 0.5 s. The EdgeTech 512 chirp sub-bottom-profiling system consisted of a source transducer and receiving hydrophones housed in a 500-pound “fish” towed several meters below the sea surface. The chirp source signal was 500–7,200 hertz (Hz) with a 30-millisecond (ms) sweep length, and record lengths were 0.35 s. These data were recorded in standard SEG-Y 32-bit floating-point format with Triton SB-Logger PC-based software that merged seismic-reflection data with differential global positioning system (DGPS) navigation data, with digital sampling of 16 kilohertz (kHz) for the mini-sparker data and 12.5 kHz for the chirp data (Sliter et al., 2009).

Water depths in the study area range from 6 m nearshore to over 300 m (Plate 1) although contour lines greater than 200 m are difficult to see above the background on Plate 1. Plate 2 shows the USGS LESS lines available for this investigation and used in other PG&E (2011a, 2011b, 2012, and 2013) reports. This survey was completed as part of the PG&E–USGS Cooperative Research and Development Agreement (CRADA), the California State Waters Mapping Program, the USGS Coastal and Marine Geology Program, and the USGS Earth Surface Processes Program. The data have been published as USGS Open-File Report 2009-1100 (Sliter et al., 2009).

The marine magnetic and the seismic-reflection data were collected synchronously. The marine magnetic data were collected during the 2008 and 2009 LESS surveys using a Geometrics G882 cesium vapor magnetometer that was towed 30 m behind the vessel in 2008 and 50 m behind in 2009. Data were collected at a 10 Hz sample rate along the nominal LESS lines at 800 m spacing. Additional shore-perpendicular magnetometer lines were run at 400 m spacing resulting in a uniform line spacing of 400 m for the magnetic data. Local base stations were established to identify and remove diurnal field variations. Data processing included smoothing to remove noise, removal of the diurnal field variations and subtraction of a reference field to create a marine magnetic-anomaly Map (Sliter et al., 2009). The marine magnetic-anomaly data are shown as an overlay on Plate 2.

### **2.3 PG&E Point Buchon LESS Data**

The Point Buchon 3D/2D data set were collected offshore of Point Buchon in 2010 and 2011 by Fugro Consultants, Inc. (FCL; 2012a). These data were acquired to support PG&E’s analysis of faults offshore of the DCP.P, including the Shoreline fault zone. The 3D data were collected at 12.5 m line spacing, and the 2D seismic-reflection data were collected at 100 m line spacing. A total of 2,019.47 kilometers (km) of 3D and 2D data were collected. Seismic lines from the northern part of this survey are shown in the southern part of Plate 2.

The data were acquired using a low-energy (1.5 kJ), high-resolution (100–700 Hz) frequency range (with a 200–225 Hz fundamental frequency) triple-plate boomer seismic



source as the acoustical source and four parallel hydrophone streamers for receiving acoustical energy. The boomer plates were towed in a sled with the source 0.3 m beneath the sea surface (FCL, 2012a). The seismic source was fired on distance (every 3.125 m), with a group interval of 3.125 m and 16 channels per streamer.

The receivers were four parallel 16-channel, 50 m long liquid-filled Geometrics GeoEel™ streamers, with GeoEel hydrophones grouped at intervals of 3.125 m (42.5 m to the first group from the head of the cable, with the center group at 25 m from the head) and towed at a depth of 2 m ± 0.5 m (FCL, 2012a; Fugro Seismic Imaging, 2012; PG&E, 2012). The 2D data were collected at 100 m spacing (see FCL, 2012b).

The Point Buchon 3D/2D data set was acquired and processed at specified standards as stated in the two survey data reports (FCL, 2012a, 2012b) and the seismic data processing report (Fugro Seismic Imaging, 2012). All three reports state that the acquisition and processing of the data were done under quality control (QC) protocols as outlined in Lekkerkerk et al. (2006) and the NCS SubSea Navigation Final Report (NCS SubSea, 2011). These data were validated under the PG&E Geosciences QA program as specified in document GEO.DCPP.TR.12.01 R0, *DCPP 3D/2D Seismic-Reflection Investigation of Structures Associated with the Northern Shoreline Seismicity Lineament of the Point Buchon Region*, and in Appendix A to that document, titled “Qualification of Point Buchon 3D & 2D Seismic Reflection Profiling Survey Data (October 2010 to February 2011)” (PG&E, 2012).

## **2.4 COMAP Alaska 1986 CDP Survey for PG&E**

In 1986, PG&E contracted with COMAP Alaska to conduct a moderate-energy multichannel seismic-reflection survey of the California State waters area from Cape San Martin in the north to San Luis Obispo Bay in the south. The objective of the survey was to provide additional control for mapping of the HFZ zone in the relatively shallow-water nearshore area. Primary survey lines were run perpendicular to the trend of the HFZ. Along the Cambria coastline, lengths varied from 6 to 10 km, and in Estero Bay, lines were up to 15 km long. Primary line spacing was a nominal 3 km. Coast-parallel tie lines were run approximately 2.5 and 5 km offshore, with an additional tie line 10 to 12 km offshore in Estero Bay. Total survey length was approximately 500 km. The COMAP survey lines used in this study are plotted on Plates 2 through 7.

The COMAP survey data source was a 160-cubic-inch water gun. The data were recorded for 2 s using a 48-channel cable. The data were processed by Seisdata Services, and included gain recovery, trace equalization, pre-filtering (20–250 Hz), deconvolution, velocity analysis every 40 shot points, normal moveout, 24-fold stacking, post-stack filtering, automatic gain control, and wave equation migration.

The data were originally recorded on tape, and stacked, filtered, and migrated record sections were provided on reproducible mylar and as SEG-Y files on tape reels. In 2009, PG&E had the taped data converted to CDs for longer-term storage. The taped and CD data records were in short (partial line) sections and had to be reassembled into single lines in the SEG-Y format for use in the IHS Kingdom program used for our interpretations (see Section 3.1). The navigation data were not with the original taped

data and had to be recovered from separate files. Unfortunately, on some lines, the navigation coordinates (given for shot points, not traces) could not be accurately coordinated with the trace headers in the SEG-Y files, and trace coordinates were interpolated for this study. For those few interpolated lines, or parts of lines, the inaccuracy in positions of specific structures (fault traces or structural axis) could range from a few meters to over 100 m. This is evident from comparison of the COMAP lines to adjacent USGS lines and from comparison with the original 1988 structure trend maps. For the parts of the lines with location problems in the SEG-Y files, paper copies of the original processed records were used as a reference. The navigation data are being re-digitized in 2014 from the original mylar base maps, and the new SEG-Y format should minimize the data coordination problems between surveys experienced earlier in this study.

## **2.5 LTSP 1988 Maps and Legacy Data**

In the mid-1980s, PG&E purchased 570 km of high-energy seismic-reflection survey data from the Western Geophysical Company (now WesternGeco, the geophysical survey business unit of Schlumberger) proprietary multi-client surveys run in 1974, 1975, and 1982. These lines extended from north of Piedras Blancas to south of Point Sal and were used in the interpretations presented for the LTSP (PG&E, 1988, 1990) and by Willingham et al. (2013). The Western Geophysical data were primarily in federal waters but did cross the HFZ in places. The data were collected using large air-gun arrays and processed to 46- to 60-fold stacks and migrated. Record length was 6.0 s. The data were provided to PG&E on tape reels and as analog sections on mylar. The analog records were used in the LTSP and Willingham et al. (2013) interpretations. Maps from those interpretations were converted to the WGS 84 coordinate system base and compared with the new interpretation based on the USGS data (see Sections 5.1 and 5.2).

Around 2010, WesternGeco released to the public all of its multi-client data from the offshore Santa Maria Basin to the USGS. This allowed PG&E to obtain SEG-Y copies of the 1974, 1975, 1976, 1978, 1979, and 1982 survey data and incorporate those data into its legacy data archive. Except for the 1976 survey data, only a few lines from these surveys lie within the area of interest of this study. However, the WesternGeco data were collected primarily for petroleum exploration with poor near-surface resolution, and they were concentrated west of the HFZ. Thus the data were of limited use for this study.

### **3.0 TECHNICAL APPROACH**

This section addresses the technical approach taken in the interpretations of the data used in this study. Software programs, data quality, criteria for interpreting structures and stratigraphy, and the accuracy limitations in mapping are discussed.

#### **3.1 Use of IHS Kingdom Program**

The IHS Kingdom Version 8.6 software program was used to view seismic-reflection data. The 64-bit copy used for this interpretation has been vetted for nuclear use at PG&E Geosciences Department office in San Francisco. The software package allows the user to view and map horizons and geologic structures on vertical seismic profiles (3D and 2D data sets, cross sections, and user-selected cross sections). The vertical cross-sectional profiles are displayed as seismic-reflection amplitudes, with the vertical axis representing two-way travel time (TWTT) and the horizontal axis representing shot points (seismic traces) and distance along the line.

Interpretations were performed on each 2D line from the Fugro 2010–2011, USGS 2008 and 2009, and COMAP86 seismic-reflection lines shown on the base map (Plate 2). Selected stratigraphic beds or layers were mapped based on one or more of the following criteria:

- Vertical sequence of distinct low- and high-amplitude reflections, either as a low-high pair (doublets) or as low-high-low or high-low-high triplets.
- Correlation over several hundred meters in lateral extent.

Angular unconformities were mapped based on one or more of the following criteria:

- Presumed younger sediments (upper reflections) overlying an angular-eroded surface of tilted/folded older rocks or reflections.
- Reflection onlap, downlap, or toplap against upper- or lower-bounding surfaces, commonly indicating a hiatus in deposition.

Faults were identified based on one or more of the following criteria:

- Abrupt lateral truncation of reflections.
- Displaced, offset, or broken reflections.
- Correlations of offset reflections across a fault plane.
- Direct fault plane reflections.
- Acoustical anomalies (e.g., presence of diffractions, especially at a reflection termination, or presence of laterally short and bright reflections adjacent to a plane that appear as “flags” or contrasting acoustic signals separated by a plane).
- Visible drag and rollover of reflections.
- Loss or substantial decrease in acoustic coherence beneath a fault plane, or distorted dips observed through a fault plane.

Fold axes were identified and mapped based on one or more of the following criteria:

- Both limbs of a fold are present, or, in the case of a monocline, beds consistently dip in one direction.
- The amplitude of the fold is greater than several tens of ms (~20 m).
- The greatest curvature of a sequence in upturned or downturned reflections.

To track faults, folds, and various horizons in the IHS Kingdom software program that were interpreted and mapped, and to correlate these with previously mapped structures, a coding scheme was used based on colors and stored on the PG&E 3D/2D IHS Kingdom project. The intent of the scheme is to recognize associations within the spatial fault patterns and map preliminary correlations of each fault identified with known fault zones (e.g., HFZ) or groups of faults (e.g., unassigned faults), associated folds, and horizons. Different colors are assigned such that each mapped structure is clearly associated with the various fault zones or groups shown on Plate 2 and discussed herein.

The color schemes used in the Kingdom program and figures presented in this report are listed below. Figures accompanying this report were produced in a GIS program. In some cases, because the Kingdom color scheme did not provide sufficient contrast in the GIS program, it was necessary to change certain colors. To be able to compare this report with the IHS Kingdom project, the colors used in the project and those used to produce the figures and plates in GIS are both called out in this report. If two colors are indicated, the first applies to the color used in the Kingdom program, the second to the color used in the report figures and plates. The following colors were used for the horizons and structures, with the IHS Kingdom colors used first, followed by colors for the figures and plates, if different (e.g., orchid/purple):

- Interpreted horizons
  - Seafloor—Dodger blue (the named color in the IHS project)
  - Seafloor multiple—Dodger blue, label only
  - Base of surficial (Holocene?) unconsolidated sediment—yellow
  - Unconformity HG1—orchid/purple
  - Unconformity HG2—gold
- Interpreted faults
  - HFZ traces—red
  - San Simeon fault zone traces—green
  - Los Osos fault zone traces—brown
  - Half Graben faults—goldenrod yellow
  - Unassigned faults—orchid/purple
- Interpreted folds
  - Anticline axis—maroon on figures /black with arrow label on maps
  - Syncline axis—blue on figures /black with arrow label on maps
  - Kink fold axis—magenta

### 3.2 Criteria for Data Quality Evaluation

The quality of individual seismic-reflection profiles used in this study varied from poor to very good, depending on resolution, data gaps, noise interference, and relative depths of imaging. The Fugro and USGS surveys used low-energy, high-frequency sources (multiplate boomer and mini-sparker) and provide very high-resolution images of the near-surface sedimentary section, but little signal penetration into the sub-sediment rock section. Record lengths were 0.45 s and 0.5 s, respectively. Depending on the subsurface geology, TWT image times ranged from 0 s over shallow bedrock to 0.3 s where there were thick sections of post-Neogene sediment. Other factors commonly affecting the quality of the high-resolution survey records are data gaps and interference from multiple reflections of the seafloor. The latter are somewhat reduced in the Fugro data because of multichannel recording and post-survey processing.

Figure 3.2-1 is an example of a mini-sparker record over shallow bedrock. It shows little sub-seafloor data except for a thin section of sediment between shot points 3650 and 3240 (offsets 5350 to 5800). Data gaps (Figure 3.2-2) may result from system crashes, equipment shutdowns due to nearby marine mammals, or interruptions due hardware maintenance. Figure 3.2-3 shows the effect of interference from seafloor multiple reflections. The thick sediment section on the northeast side of the Half Graben fault (discussed in Section 4.4) is partially obscured at depth by the seafloor multiple, and the HG2 unconformity (mapped for this study) cannot be continued to the fault.

The COMAP and Western Geophysical surveys used higher-energy and lower-frequency energy sources (water guns and air guns). They have less near-surface resolution of reflections and small-scale structures, but offer increased image depths (1 to 2 s or more) into the sediment and Neogene sedimentary rocks in our study area. The Western Geophysical records provide even greater depth imaging further west of our study area, into the offshore Santa Maria Basin. The effect of seafloor multiples has been reduced in many areas because both of these surveys were multichannel and subject to post-survey processing.

Plate 3 shows the portions of the USGS and COMAP lines that have their depths of imaging limited to the surficial sediment (Holocene?) layer and provide little or no data on the continuity of subsurface structures. The background imagery of the plate is a multibeam bathymetry, and areas of bedrock outcrop are outlined in green. The shiptrack lines are highlighted in yellow where imaging is limited to the surficial sediment layer and where there are data gaps. A comparison of Plate 2 (Regional Structural Trends) and Plate 3 (Limited Data Areas) highlights the overall effect that near-surface bedrock has on the ability to map structural continuity over much of the project area.

### 3.3 Criteria for Mapping Structural Trends

The criteria for identifying and mapping geological horizons and structures on the 2D seismic-reflection profiles using the IHS Kingdom program are listed in Section 3.1. The limitations in recognizing subsurface structures imposed primarily by shallow bedrock and data gaps are summarized in Section 3.2. Two other criteria were applied in

constructing the structural trends maps (Plate 2 at 1:50,000 scale and Plates 4, 5, and 6 at 1:25,000 scale):

1. The specific geological feature, whether fault trace or fold axis, had to be confirmed by both authors. Initially this was done separately, but later the actual location and depth range on the seismic-reflection profiles were confirmed by consensus.
2. The structure had to be identified on two or more adjacent lines. The Neogene and earlier sedimentary, volcanic, and metamorphic rocks on the shelf in the study area are highly deformed. Apparent fault traces may be only a few tens of meters apart, and folds may have wavelengths of 100 m or less. It is not uncommon to see a fault or fold on one line and not recognize the structure on adjacent lines only 400 to 800 m apart.

Figure 3.3-1 is an example of small-scale discontinuous structures. We have interpreted three possible faults in a 200 m wide section of the seismic-reflection profile and another possible fault 250 m to the northeast. There may be other fault traces and folds present in the same area, but they are not identifiable by us. While the two bounding faults are recognized in profiles (on lines) to the north and south, the intermediate structures are not exhibited on adjacent lines. Figure 3.3-2 is also an example of closely spaced structures—in this case, three folds between two faults. A syncline interpreted between two folds may also be a fault. It is present on the immediately adjacent COMAP Line 47, but not on the two USGS lines to the north and south, and it is not shown on the structural trend map. This figure also shows diffractions in the vicinity of the Half Graben fault zone (yellow) and other apparent fold reflections below 0.22 s at the left of the figure. The latter do not appear to correspond to the shallower structures and may be out-of-plane reflections. Figure 3.3-3 is an example of the lack of resolution of shallow features in the COMAP data, which limits their use in correlations with the high-resolution data; this is discussed in Section 3.4.

### **3.4 Accuracy Limitations in Mapping Structural Trends**

The accuracy to which the location and continuity of a specific geologic structure can be depicted on the maps in this report is dependent on several factors:

- Accuracy of the seismic-reflection and bathymetric surveys offshore navigation systems.
- Accuracy of the processed data relative to the assigned coordinates.
- Resolution of the geologic feature in the SEG-Y files used in the IHS Kingdom program or seafloor features in the GIS files.
- Data spacing (survey line spacing and/or bin size).

The MBES data and data from the USGS 2D seismic-reflection survey and Fugro 2D and 3D seismic-reflection survey were all positioned using DGPS navigation systems, the WGS 84 datum, and UTM Zone 10 N coordinates in meters. The high-resolution bathymetry and seismic-reflection systems recorded positioning data at nominal intervals

of a few meters along the survey lines. The accuracy of individual position measurements is on the order of a meter or better. Processing of the data into bins (MBES and 3D seismic-reflection) or traces (2D seismic-reflection) recorded with a towed multichannel hydrophone may further reduce the location accuracy of the processed data. The MBES systems generally have minimal layback, and the location degradation is primarily related to the water depth of the seafloor being imaged. For 2D or 3D seismic-reflection data, processed location accuracy depends on the accuracy to which the hydrophone steamers (cables) have been recorded and modeled in the processing. Thus the accuracy of the coordinates for a series of seismic traces may vary from a few meters (bin size) to as much as a few tens of meters relative to true geodetic location. The USGS estimates that for the 2008–2009 surveys, “the horizontal data thus linked to [a] ship’s position is estimated to be within 30 meters” (Sliter et al., 2009).

The 1970 to 1980s high-energy seismic-reflection data were positioned using shore-based range-range systems with stated accuracies of  $\pm 3$  m nearshore and  $\pm 5$  to 10 m when 15 km offshore. The longer recording intervals and the longer towed hydrophones resulted in further reduction in the processed data relative to actual geodetic position. These data were generally referenced NAD 27 and converted to WGS 84 for this study. Comparison of coordinates of specific seafloor or structural features from these earlier surveys to the same features imaged by the post-2000 bathymetric and seismic-reflection surveys commonly indicates location differences of 20 m to over 100 m as viewed in the IHS Kingdom program.

Another factor affecting line-to-line (profile-to-profile) correlations of geological structures is the resolution of the feature on the seismic-reflection profiles. In the high-resolution Fugro and USGS seismic-reflection data sets, fault locations and structural axes can often be picked (resolved) within 10 to 20 m, although the stated vertical resolution of the data is 1 m (see Table 2.1 of PG&E, 2014), based on a frequency range of approximately 200–1,600 Hz (Johnson and Watt, 2011). However, on the higher-energy COMAP lines, the same feature, if recognizable, may not be resolvable to within 20 to 40 m or more (see Table 1 of Willingham et al., 2013). (Note that the near-surface geological structures are often not discernible on the higher-energy data because shooting and recording parameters were designed for deeper targets.) These minor differences in locations associated with position inaccuracies or resolution problems lead to a scatter of picks (interpretive locations) when the locations of a specific structure on a series of seismic-reflection profiles are projected onto a map.

Interpreted line-to-line continuity of structural features is also highly dependent on data (line) spacing. As discussed in Section 5, the 400 to 800 m line spacing of the USGS high-resolution seismic-reflection data resulted in different correlations of fault traces and structural axes than the nominal 3 km spacing of the COMAP86 lines used in the LTSP. However, even with the 400 to 800 m line spacing of the USGS survey, many structures are apparently of shorter horizontal extent and are observed on only one or two seismic-reflection profiles. This, along with the conditions described above, often provides the interpreter with alternate correlations when extending structural feature alignments on maps. It should be expected that other interpreters might occasionally establish alternate correlations, trends, and lateral extents for geological structures in our study area.

## 4.0 INTERPRETATIONS AND ANALYSES

In this section, we present our interpretations and analyses of the seismic-reflection data sets used for this study. We focus primarily on the major fault zones of the Point Buchon–Estero Bay–San Simeon Point region, which includes the HFZ, San Simeon, and Los Osos fault zones. The area also includes the newly named Half Graben fault zone, which trends between the HFZ and the San Simeon faults, and several zones of minor faults that are not assigned names but simply labeled “unassigned faults.” Two of these groups of “unassigned faults” are discussed further, one in the area between the HFZ and the Piedras Blancas antiform, the other offshore of Islay Creek at the south end of Estero Bay.

For each of the fault zones, we discuss the geometry, continuity, association with adjacent zones, evidence for recent fault activity based on offsets of acoustic horizons and associations with recorded seismicity and magnetic anomalies.

The bases for our discussions are presented as structural trend maps and figures illustrating selected sections of seismic records. The regional structural trends shown on Plate 2 include the entire study area at 1:50,000 scale. The structural trends are presented in greater detail at 1:25,000 scale on Plates 4, 5, and 6 for the southern, central, and northern areas of the study, respectively. The background for the structural trend maps is the onshore DEM and offshore MBES data. Earthquake epicentral locations are shown as overlays on Plates 4, 5, and 6. Magnetic anomaly data are shown as an overlay on Plate 2.

The figures illustrate the interpreted fault zones and associated structures, primarily folds, on the seismic sections at various scales. An uninterpreted section is shown at the top half of the figure and an interpreted section is at the bottom half. The location and extent of the figures are shown on all plates containing the illustrated seismic section.

### 4.1 The Hosgri Fault Zone

The HFZ trends subparallel to the south-central California coast for over 110 km from south of Purisima Point to north of Point Estero and forms the eastern margin of the present offshore Santa Maria Basin (PG&E, 1988; Willingham et al., 2013). The HFZ has long been considered part of the coastal California fault system that also includes the San Simeon, Sur, and San Gregorio fault zones to the north (Hall, 1975; Graham and Dickinson, 1978; Silver and Normark, 1978; Dickinson et al., 2005). Based on analysis of geomorphic and structural features along its entire length, the HFZ has been characterized as an active 110 km long convergent, right-oblique slip (transpressional) fault zone with identifiable northern and southern terminations (Willingham et al., 2013).

#### 4.1.1 *The HFZ—Point Buchon to Offshore Cambria*

Within our study area, mapped traces of the HFZ extend northwest from offshore of Point Buchon for approximately 37 km to a point approximately 7 km offshore from the coastline at Cambria (Plates 2, 4, 5, and 6). This part of the HFZ was termed the “Northern Reach” in Willingham et al. (2013) and PG&E (1988). Near the northern termination, we observe slope failures resulting from possible gas migration and fluid



discharge (increased pore pressures) along the westernmost trace of the fault. These features are described in Section 4.1.2.

At the south end, the HFZ trends about N30°W. Approximately 23 km north, opposite Point Estero, the HFZ bends to the northwest and trends N37°W. Throughout the mapped area, the HFZ consists of multiple strands, some of which disrupt the seafloor or a very shallow sediment section, and some of which are buried by 5 m or more of undisturbed sediment. Buried traces are indicated by dashed lines in the structural trends maps (Plates 2, 4, 5, and 6), and surface and near-surface traces are indicated by solid lines. Evidence of Holocene activity varies along the length of some traces and transfers between adjacent traces. Between traces are local areas of both restraining and releasing bends.

Figures 4.1-1 through 4.1-7 are illustrations of seismic-reflection profiles across the HFZ. Figure 4.1-1 is west of Point Buchon and Figure 4.1-4 is west of Point Estero. The northern 9 km of the HFZ are illustrated on Figures 4.1-5 through 4.1-7. Figure locations are shown on the study area index map (Figure 1.2-1) and the plates.

Figure 4.1-1 (USGS Line PBS-21) shows two interpreted strands, the central and eastern strands, of the HFZ offshore from Point Buchon. Both strands are documented on the Fugro and USGS survey seismic-reflection profiles in this area. The seafloor outcrop (apparent scarp) associated with the central strand is approximately 10 m high and 1 km long; it is evident in the MBES data just above the southern border on Plate 4. These features are also illustrated on Figures 11A and 11B of Johnson and Watt (2012). These authors interpret the flat-lying sediment horizons on the west to be Holocene and late Quaternary in age and the folded rocks to the east to be inferred Neogene bedrock. They do not show the eastern strand of the HFZ, which we interpret to be present based on the thinning and apparent termination of a thin Holocene sediment layer visible on this and other profiles in the area and on the apparent termination of subsurface fold limbs observed in the Fugro 3D/2D survey data. Interpretation of folds and possible additional faults in the shallow bedrock area east of the central strand is difficult because of limited signal penetration into the tightly folded bedrock.

Figure 4.1-2 (USGS Line PBS-43) is approximately 10 km north of Figure 4.1-1 in an area of seafloor bedrock exposures wedged between the HFZ and an unassigned fault on the east. (Unassigned faults are those that have not been previously named in PG&E reports.) The latter fault has a more westerly trend (N60°W–N70°W) than the HFZ (Plates 2 and 4). The outcrop area is interpreted to be the result of interaction between the HFZ and one or more of the unassigned faults trending toward the HFZ from the southeast. The central fault strand at the west end of the outcrop area is the same strand exhibited at the western edge of the outcrop on Figure 4.1-1, 10 km to the south. The buried strand on the west is mapped to veer to the southwest. It may correspond to a buried strand mapped southwest of Figure 4.1-1, but the continuity could not be established with the data used in this study.

A seismic-reflection profile (USGS Line PBS-43) is shown on Figure 12B of Johnson and Watt (2012) that illustrates similarities and differences in interpretations. These authors' interpretation and our interpretations are similar, with just a few minor differences, as follows:

- Where Johnson and Watt (2012) interpret “sediment drape over bedrock sliver” in the zone, we attribute the bright spot to gas on the west side of the HFZ. In actuality, it could be both.
- Johnson and Watt (2012) interpret a fault on the east side of the small central outcrop (at about shot point 9800 on the profile) that we had not mapped. This corresponds with the edge of a short ridge on the MBES data (Plate 4). The fault is not long enough to meet our mapping criteria (Section 2) and it may have a strike similar to the unassigned fault rather than to the HFZ.
- The eastern fault that Johnson and Watt (2012) interpret as the central strand of the Los Osos fault is on trend with our designated strands of the Los Osos fault zone to the northeast; however, we cannot trace it to near the shoreline where the Los Osos has been mapped onshore. The fault is nonetheless within the broad area designated as the “offshore projection of the Los Osos fault” in the maps accompanying the LTSP reports (PG&E, 1988, 1990).

Figure 4.1-3 (USGS Line PBS-08) is approximately 2.5 km north of the USGS line shown on Figure 4.1-2. This line is shown on both Plates 4 and 5. The profile shows five fault strands, but only three appear on the maps:

- The westernmost buried strand (shot point 2125).
- The central strand associated with a seafloor slope change (shot point 2440).
- The dipping strand on the eastern side of the outcrop (shot point 2870).

All three strands are correlated with similar features shown on Figure 4.1-2 and Plate 4. The eastern strand forms the western boundary of a 1.5 km wide basin between the HFZ and the Los Osos fault zone to the east. The uplifted block between the central and eastern strand shows no interpretable reflections indicating either steep dips or non-stratified rock. Johnson and Watt (2012) show a seismic-reflection profile (Line PBS-40, 835 m south of Line PBS-08) with features similar to those shown on their Figure 12C. Our interpretation is similar to theirs except that they show the dipping surface as a basement slope associated with an anticlinal structure that would correlate with the outcrop at shot point 2800 exhibited on Figure 4.1-3.

Figure 4.1-4 is a seismic-reflection profile (USGS Line PBS-230) and is located 13 km northwest of Figure 4.1-3 (Plate 5). The trend of the HFZ bends westward at this location but appears continuous, with several traces of the fault zone to the south. The MBES data images minor seafloor slope changes associated with the three strands, indicating the HFZ is still active in this area. At the right of the profile is a gentle anticlinal fold that is either faulted or sharply folded on the eastern flank. We have informally named such a feature a gentle “kink fold,” as it can be traced to the north, where it is obviously a folded limb of the anticline and not a fault. Farther north, there are slope failures or mass wasting features along the HFZ. These features, which are discussed in Section 4.1.2, do not necessarily correlate with the buried traces of the HFZ; they are probably caused by gas or fluid migrating upward along the buried fault planes.

Offsets of the seafloor and shallow sediment horizons are the primary criteria used to identify HFZ strands that have been active in the Holocene. Earthquake epicenter data

(Plates 4, 5, and 6) are another indication of recency of activity, although not as site-specific since the epicenters are at depths of 2 to 10 km and the dips of the individual strands to those depths are not imaged. Along the HFZ, scattered epicenters are plotted west of Point Buchon and Morro Bay; a few more are plotted west of Point Estero. However, north of Point Estero, the epicenter plots move to the eastern strands of the HFZ and onto areas associated with unassigned faults that are on trend with the HFZ (Plates 5 and 6).

Positive marine magnetic anomalies (Plate 2) are generally interpreted as indicators of shallow basement rocks, in this case the Franciscan Complex rocks and/or intrusives. The primary area of positive magnetic anomalies near the HFZ is the broad high extending along the Los Osos fault zone strands as they approach the HFZ. North of Point Estero the positive magnetic anomalies trend more northeasterly and veer away from the HFZ.

#### ***4.1.2 Fluid-Induced Slope Failures Along the Western HFZ Trend***

The recently collected USGS MBES data show unique seafloor morphology along the distal edge of the continental shelf in the west-central part of the study area (Plates 1, 2, and 5). Unlike the majority of the shelf, which exhibits a smooth seafloor, or the nearshore areas and west-central Estero Bay, where bedrock exposures exist, the area near the shelf break is hummocky, with long linear ridges and depressions oriented parallel to the shelf break. The shelf break here has a sharp relief and is very linear, trending northwest-southeast and appearing as a prograding shelf edge. The shelf is probably controlled by faulting associated with the HFZ, as several fault strands are mapped in this area (Plate 2; Figures 4.1-1 through 4.1-4) that extend to or near the seafloor, with seafloor expression along one strand.

The very linear shelf break is broken in several places, with prominent mounds and depressions shoreward on the shelf, and subtle sediment gravity-flow failures seaward on the upper slope. Two prominent and one subtle depressions notch the shelf break southwest of Cambria, with the larger of the two prominent depressions located in the south (Plate 5). However, no fault is observed in the seismic-reflection profile (USGS Line PBS-235) in the area where this larger depression exists and a well-developed downslope lobe has formed. Here, steeply westward-dipping rhythmically layered reflections intercept the seafloor or are covered with a thin layer of surficial sediment (Figure 4.1-5). Strands of the HFZ are discontinuous through the area but appear as deep strands beneath the smaller, more northerly located depression (Figure 4.1-6). The acoustic nature of the shallow subsurface in the vicinity of these depressions exhibits transparency and chaotic reflections that indicate slumping and downslope movement.

A major westerly strand of the HFZ appears to control the morphology of the outer shelf from west-central Estero Bay, where the unassigned fault zone (HFZ transitional faults trending toward the Piedras Blancas fault and fold belt) impinges on the HFZ in the south to just west of Cambria in the north (Plates 2 and 5). Along this margin the faults of the fault zone exhibit pockets or lenses of high-amplitude reflections (“bright spots”) that most likely represent gas trapped along fault planes or between faults (Figures 4.1-2,

4.1-3, and 4.1-6). These bright spots are present along the faults that lie beneath the prominent southern depression and along faults to the south and north of this depression.

Hovland and Judd (1988), Yun et al. (1999), and Eichhubl et al. (2002) have described the relationship of bright spots to the presence of gas. In areas where gas was detected in seismic-reflection profiles in the Santa Barbara Channel, fluid-flow-induced morphology was imaged in MBES data and observed in situ using a remotely operated vehicle (Eichhubl et al., 2002; Greene et al., 2002). Mass wasting along the eastern flank of the Santa Barbara Channel appears to have been induced by fluid flow (Greene et al., 2002), resulting in top-down slumping (fluid-induced sediment mobilization initiated at the upper slope) and sediment flow (see Pratson et al., 1994). Subsurface fluid flow of gas and water migrating up along faults appears to have played a major role in the geomorphologic formation of the distal part of the continental shelves in the Santa Barbara Channel, in the Point Conception–Point Arguello offshore area, and along the northern Monterey Bay outer shelf. All of the locations are associated with bright spots observed in seismic-reflection profiles (Mullins and Nagel, 1982; Nagel et al., 1986; Greene et al., 1999, 2002).

Greene et al. (1999, 2002) describe fluid-induced morphologies of scallops and collapsed canyon heads (e.g., Ascension and Año Nuevo Canyons north of Monterey Bay and Conception and Arguello Canyons offshore of Point Conception) that are present along the distal edge of the shelf and on the upper slope. The shelf and upper slope of each of these areas are associated with faults that bound a hydrocarbon-source basin (i.e., the Santa Barbara, offshore Santa Maria, and outer Santa Cruz Basins). Thus gas and fluids migrate from deep in the basins to the surface along fault conduits (Hoskins and Griffiths, 1971; McCulloch, 1987, 1989; Greene et al., 1999, 2002).

Not only do surface gravity flow and subsurface fluid flow destabilize slopes through increased pore pressures and cause mass downslope movement, but methane discharge at the seafloor forms mounds of authigenic carbonate. This reaction is consistent with pulses of rapid gas discharge that result in fluidized entrainment of mud (Brown, 1990) and formation of mud volcanoes (although no mud volcanoes are identified in this study). In the Santa Barbara Channel, episodic movement of formation fluids along faults from the Monterey Formation to the surface has been inferred by Eichhubl and Boles (2000a, 2000b). Authigenic carbonate mounds and ridges can be formed at the seafloor by formation fluid, including diagenetically altered connate formation water, gas, and oil, or by shallow microbial gas formed by bacterial methanogenesis (Eichhubl et al., 2002). Carbonate mounds and slabs have been reported from Coal Oil Point and the Mid-Channel trend, and along the fault scarp of the Point Conception fault in the Santa Barbara Channel (Eichhubl et al., 2002).

Morphologic features along the continental shelf edge between central Estero Bay and offshore of Cambria appear similar to those authigenic carbonate mounds, ridges, and slabs that exist elsewhere along the California coast and are associated with hydrocarbon basins. Therefore, it appears that the HFZ in the area of this investigation has acted as a conduit for fluid flow from deep in the offshore Santa Maria Basin to the seafloor. Gas appears to be trapped up against the faults of the fault zone, as evidenced by bright spots

and past escaping of fluids at or near the seafloor that appear to have formed authigenic carbonate ridges and slabs (Plates 2 and 5). Depressions and linear troughs associated with the gas-charged faults appear to represent mass failure at the top of the continental slope where subsurface fluid flow mobilized sediment, resulting in excavation beneath the shelf edge and sediment flow downslope to form the subtle lobate structures observed in the MBES bathymetry (Figure 4.1-7 and Plate 5). This morphology is not unlike that described by Greene et al. (1999, 2002) for the Ascension slope north of Monterey Bay, and the collapse canyon and gully heads described by Eichhubl et al. (2002) and Greene et al. (2002).

#### **4.2 The HFZ Transition to the Piedras Blancas Fault and Fold Belt**

A series of unassigned en echelon fault strands step northwestward from the north end of the central segments of the HFZ, specifically from the eastern strands of the HFZ, faults labeled H-E2 and H-E3 (Plate 6). To the west, the recent western traces of the HFZ, faults H-W and H-E1 (Figure 4.2-1) end and appear to transition into a kink fold that in turn trends into a syncline and anticline pair that represents the south end of the Piedras Blancas fault and fold belt (Figure 4.2-2; Plate 6). The transitional fault zone (labeled UH-1 to UH-6 on Plate 6) between the northern HFZ and the faults and folds of the Piedras Blancas antiform lies between the kink fold and the San Simeon fault zone (Figure 4.2-3). These faults exhibit similar strike to the HFZ to the south and west and extend northwestward to where the more westward-trending eastern strand of the Piedras Blancas fault is imaged in the bedrock exposure offshore and west of San Simeon Point (Plate 6).

The eastern strand of the Piedras Blancas fault zone (fault PB-E) is a bedrock fault that is well defined by the truncation of eastward-dipping, rhythmically layered reflections that juxtapose steeply westward-dipping reflections (Figure 4.2-4). At this location, fault PB-E does not appear to offset the bedrock surface or the thin layer of overlying unconsolidated sediments. To the west of the fault, the eastward-dipping reflections crop out on the seafloor to form a bedrock exposure. West of this bedrock exposure, a thin (up to 20 m) layer of flat to gently dipping reflections covers an irregularly eroded bedrock surface. The bedrock here varies from folded to westward steeply dipping reflections that are folded into a syncline near the west end of USGS Profile PBS-227 (Figure 4.2-4). An anticline and the central strand of the Piedras Blancas fault zone are also exhibited in the profile.

The western strand of the Piedras Blancas fault zone is buried beneath westward-dipping reflections of well-layered sediments of probable Pleistocene age (Figure 4.2-5). This fault juxtaposes well-layered westward-dipping reflections on the west with folded rhythmically layered reflections to the east. Two well-formed anticlines with an intervening syncline are imaged on USGS Profile PBS-224 (Figure 4.2-5). A distinct angular unconformity exhibits the erosion that has truncated the folds, and a thin (~20 m) layer of unconsolidated (probable late Holocene) sediment, which thins to the west, and overlies the flat bedrock surface.

In the north end of our study area where the eastern and central strands (faults PB-E and PB-C) appear to deform bedrock (Figure 4.2-6; Plate 6), we observe a style of structural deformation similar to the one described above for the southern and central parts of the Piedras Blancas fault and fold belt. Here, the eastern strand of the fault zone appears to control the western boundary of the bedrock exposure and displaces the bedrock surface and overlying westward-dipping reflections overlying the bedrock surface. To the west of the two fault strands, a broad anticline is imaged in the seismic-reflection profile (Figure 4.2-6). Both faults and the anticline are truncated along an angular unconformity that underlies a thin (up to 20 m thick) cover of flat-lying reflections (probable Holocene sediments).

Only the southwest flank of the Piedras Blancas antiform is included in this study area. High-energy seismic-reflection profiles from petroleum exploration surveys show dated unconformities across both the offshore northwestern and southwestern flanks (Willingham et al., 2013). These profiles suggest that the folded and faulted rocks imaged on Figures 4.2-4 through 4.2-6 are of Miocene or older age, and that the structures formed above detachments at subsea depths of 0.8 km or more (1.0 s and greater TWTT) as shown by Willingham et al. (2013). Therefore, the detachments lie beneath the maximum TWTT of the USGS records on Figures 4.2-2 through 4.2-6. This suggests that the folds and faults imaged on the USGS seismic-reflection profiles may represent relatively shallow deformation associated with only minor basement involvement. Earthquake epicenters in the Piedras Blancas area are generally at depths of 4 km or more and apparently are not directly associated with the near-surface structures (Plate 6). Farther southeast, in the transition area between the HFZ and Piedras Blancas structures, there are apparent associations between some of the faults labeled UH-1 to UH-6 and epicenters at depths of 2 km and more.

### **4.3 The Los Osos Fault Zone**

The Los Osos fault zone is interpreted to extend offshore into Estero Bay from its mapped location onshore near Morro Bay. This fault zone is characterized in the seismic-reflection profiles as four strands in the nearshore area, reducing to two strands to the northwest, a continuous northern strand and a discontinuous central strand (Plates 2 and 4). In the southeastern part of the fault zone, the individual strands bound a block of chaotic and deformed reflections (Figure 4.3-1). Within approximately 7.5 to 9 km from the shoreline, the four strands have apparently been reduced to a single northern strand (Figure 4.3-2). The apparent vertical displacement on the northern strand is down to the northeast, with a minimum vertical separation of 20 and 15 m interpreted on Figures 4.3-1 and 4.3-2, respectively. Approximately 16 km from the shoreline, the fault-bounded block between the central and northern strands appears as an antiform horst (Figure 4.3-3), down on the north along the northern strand and down on the south on the southern strand. The surface of the antiform is erosional, shallowly buried beneath onlapping surficial and older sediments forming an angular unconformity (Figure 4.3-2).

As mapped on Plates 2 and 4, the Los Osos fault zone extends for over 18 km northwestward from near the shoreline at the south end of Morro Bay to near the southern terminus of the Half Graben fault zone located on the outer continental shelf southwest of

Point Estero (Plate 4). The most complex part of this fault zone lies along its eastern half, where bedrock is shallowly buried beneath a variable thickness (~20–30 m) of surficial sediment and composed of four different fault strands. Between the primary northern and southern strands, folds and secondary faults trend parallel to the primary strands. This eastern part of the fault zone parallels the many strands of the unassigned fault zone discussed in Section 4.6 below. One or more strands of the unassigned fault zone have been included in the Los Osos fault zone in previous mapping (PG&E, 1988; Willingham et al., 2013; Johnson and Watt, 2012).

To the northwest, the fault zone appears less complex, composed of only the two primary strands, and although the fault trends toward the Half Graben fault zone and the HFZ, no distinct connection was observed in the data. Here, the fault zone is buried beneath a thicker sequence of sediments than in the east, which may contribute to observing less complexity in the structures.

Recorded earthquake epicenters are plotted on Plate 4. They are more numerous, and deeper, at the southeast end of the fault and diminish in number and depth to the northwest. The epicenters do not lie directly over the surface fault traces, which suggests that the fault strands may dip or coalesce at depth.

The strands of the Los Osos fault zone overlie a magnetic high that trends northwest offshore from the Irish Hills into the southern part of Estero Bay (Plate 2). The magnetic high is bounded on the southwest side by a series of unassigned faults (Section 4.6) and to the northwest by the HFZ. This magnetic high is in an area of bedrock outcrops. Although there are Franciscan Complex outcrops in the Irish Hills, the offshore outcrops identified by bottom samples and cores have been primarily identified as Miocene “type” or “age” sedimentary units (Willingham et al., 2013, their Plate 2 and Table 4). The magnetic anomalies may be associated with slivers of Mesozoic ultramafic rocks beneath the Miocene sedimentary rocks, similar to the onshore outcrops.

#### **4.4 The Half Graben Fault Zone Offshore of Cambria**

The “Half Graben fault zone” is an informal name we apply to the fault zone that trends N20°W to N25°W from its intersection with the HFZ southwest of Point Estero (Plates 2 and 5). It is on trend with the offshore segment of the San Simeon fault zone (Section 4.5) but does not make a direct connection with it (Plate 6). The Half Graben faults are shown in yellow on Plates 2, 5, 6, and 7 and Figures 4.4-1 through 4.4-6. The main western strand of the fault zone exhibits down-to-the-east normal offset. The apparent “acoustic” basement rises gradually to the east, and the sediment section thins and onlaps bedrock outcrops that form the shallow shelf offshore from the relatively straight section of the coastline extending south of San Simeon Point to Point Estero (Plates 2, 5, 6, and 7). The inverted triangular shape of the sediment basin bounded by the western strand of the Half Graben fault zone, together with the apparent lack of a fault bounding the eastern side (Figures 4.4-2, 4.4-4, and 4.4-5), is the source of the informal name.

Segments of the Half Graben fault zone were mapped in previous interpretations based on the analysis of high-energy multichannel-exploration-type seismic-reflection data (PG&E, 1988, 1990; Willingham et al., 2013). These normal fault segments were

interpreted as part of an extensional “pull-apart” basin developed as a step-over feature between the two right-lateral strike-slip faults, with the HFZ on the west and the interpreted southeast extension of the San Simeon fault along the relatively straight coastline between San Simeon Point and Point Estero (DiSilvestro et al., 1990; Lettis et al., 1990; Hanson et al., 2004). The USGS seismic-reflection profile and magnetic surveys in 2008 and 2009 provided increased data density and resolution along this structure and allowed for mapping the continuity of the western strand and basin over a 13 km length. These data also provided evidence of the direct association of the south end of the western strand with the HFZ. Johnson and Watt (2012) consider the western strand of the Half Graben fault zone to be the eastern strand of the HFZ. We consider the Half Graben fault zone to be a separate structure because its trend is 10 to 20 degrees northeasterly of the general HFZ trend in the area north of Point Buchon, and the apparent sense of slip is normal rather than right-oblique strike-slip.

Figures 4.4-1 through 4.4-6 show seismic images of the Half Graben fault zone and the associated basin. Locations of the figures are shown on Figure 1-1 and Plates 1 through 7. Figure 4.4-1 is located in the southern part of the zone and Figure 4.4-6 is located in the northern part. We have mapped two unconformities within the basin, HG1 and HG2. Horizon HG1 is a shallow unconformity indicated in orchid (light purple) in the figures and maps. Where HG1 overlaps the top of the fault outside the basin, it corresponds with the base of the shallow or surficial sediment (Holocene) section. Horizon HG2 (indicated in gold on figures and maps) is the apparent “acoustic” basement for the USGS 2008–2009 mini-sparker survey data. It probably represents the top of the deformed Neogene rocks in the eastern part of the basin but cannot always be traced to the western strand because of insufficient signal penetration and interference from seafloor multiple reflections.

Figure 4.4-1 is an example showing the western strand of the Half Graben fault zone and two unconformities. Horizon HG2 cannot be mapped west of shot point 3300 for the reasons stated above. The minor swale in the horizon at shot point 3300 and TWTT of 0.2 s may represent a small fault. Figure 4.4-2 (CM Line 47) is an adjacent line to USGS Line PBS-209 (Figure 4.4-1) and is a seismic-reflection profile collected during the COMAP 86 water-gun survey. The COMAP data have less resolution but greater image depth than the USGS data. The HG1 unconformity is difficult to resolve in the COMAP data, but the HG2 unconformity can be traced to the western strand where it is interpreted to be at a depth of 0.42 s TWTT on Figure 4.4-2 (~224 m below the seafloor; Plate 7). (Note the band of noise above the seafloor reflector on the COMAP data is a result of compositing into SEG-Y files and does not appear on mylar or paper copies of the profiles.)

Figure 4.4-3 (USGS Line PBS-230) crosses the Half Graben fault zone northwest of Point Estero. The top of the fault in this area is overlain by almost 10 m of apparently undisturbed Holocene sediment. The acoustic basement is considerably shallower than is shown on Figure 4.4-2. The diffractions beneath the western part of HG2 are interpreted to represent intra-basin faults that do not extend into the sediment section above HG2 in this area. The location of Figure 4.4-4 (USGS Line PBS-233) is approximately 2 km north of Figure 4.4-3 (USGS Line PBS-230). The HG1 unconformity is thinner but still



overlaps the top of the fault strands. The acoustic basement remains relatively shallow. Additional fault(s) within the basin extend above the acoustic basement into the sediment section.

Figure 4.4-5 (USGS Line PBS-236) is slightly less than 2 km north of Figure 4.4-4 (USGS Line PBS-233). The prominent seafloor scarp seen on the multibeam data (Plate 5) is the southern part of the west strand of the Half Graben fault zone. Movement along faults internal to the basin has deformed the HG1 unconformity. The seafloor multiple obscures the HG2 reflector, but based on the diffractions, it may exist at relatively shallow depths. The basin narrows to the north, and the slope of the eastern side of Horizon HG2 is steeper. Figure 4.4-6 (USGS Line PBS-261) is less than 2 km north of Figure 4.4-5 (USGS Line PBS-236). The acoustic basement is shallow, immediately beneath the HG1 unconformity. This is the northernmost line that shows the seafloor scarp.

Plate 7 is an isopach map showing the thickness of the sediment section within the Half Graben basin. The widening and deepening of the sediment section from north to south is evident in the contours. At the south end of the Half Graben fault zone, an anticlinal ridge and the north end of the Los Osos fault disrupt the basin, and the sediment here onlaps the eastern flank of the anticline. The sediment section on the western flank of the anticline to the HFZ is thicker than shown in the contours, but the HG2 unconformity cannot be recognized in this area. Figure 4.3-3 across the Los Osos fault zone shows the anticlinal structure and HG-2 on the east, and the Los Osos fault extending into the basin on the east side of the anticlinal structure.

Earthquake epicenters plotted on Plate 5 suggest that the fault may extend to depth with a slight eastward dip as suggested on Figure 4.4-2. The epicenters are shallower, 4 to 6 km at the south end of the fault, and increase in depth toward the north end of the fault. Both the epicenter data and the seafloor escarpment suggest the fault is still active.

The magnetic anomaly trend along the northern part of the Half Graben fault is parallel to ultramafic rock bodies within the Franciscan Complex onshore. Core samples collected on the seafloor outcrops associated with the fault zone in this area were identified as sandstone and shale of undetermined age. Diver samples and observations of the outcrops along the coast between Point Estero and Cambria were similar in lithology to the onshore Cretaceous rocks in this area (Willingham et al., 2013).

#### **4.5 The “Cambria Gap” and the San Simeon Fault Zone**

The HFZ and the San Simeon fault zone have long been considered parts of the coastal California fault system that also includes the Sur and San Gregorio fault zones to the north. The following papers all refer to the coastal California fault system:

- Hall (1975)
- Graham and Dickinson (1978)
- Silver and Normark (1978)
- Dickinson et al. (2005)
- Johnson and Watt (2012)

- PG&E (1988, 2012)
- Willingham et al. (2013)

Geologic and geophysical evidence for the physical nature of the association between the HFZ and the San Simeon fault zones has been addressed in only a few papers, however, and there has been no general agreement on the subject. Leslie (1981) proposed the connection using late 1970s and early 1980s USGS high-resolution seismic-reflection data and aeromagnetic data, but still had to infer a direct connection because of the lack of definitive data along a section of the seismic survey. DiSilvestro et al. (1990) and Lettis et al. (1990) used data from the LTSP (PG&E, 1988) to propose that the association between the faults was across a pull-apart basin. Their pull-apart basin is the half-graben basin discussed above. This model inferred that the San Simeon fault continues south along the coastline to Point Estero. Recently, Johnson and Watt (2012) used the USGS 2008 and 2009 LESS data and marine magnetic data (Plate 2) to infer a direct connection between the eastern strand of the HFZ, the Half Graben fault (which they consider the extension of the eastern strand of the HFZ), and the San Simeon fault. In this section we examine the evidence for a direct connection using the USGS LESS data.

Between the north end of the Half Graben fault zone (Section 4.4) and the south end of the San Simeon fault zone to the north is a 7 km long gap where evidence of recent faulting is lacking (Plate 6). We use the term “Cambria gap” as an informal designation to facilitate correlation between maps, figures, and text. Based on the data interpreted for this study, weak to moderately strong reflections observed within the thin (up to 20 m thick) unconsolidated sediment that overlies the shallowly buried bedrock surface are undeformed in this gap area (Figures 4.5-1 through 4.5-4). Figure 4.5-1 is 2.5 km north of the last line (USGS PBS 260), where we find evidence of the Half Graben fault. The projection of a direct line between the Half Graben fault and the San Simeon fault’s western trace would cross USGS Line PBS 256 between shot points 600 and 700. Although the record is not clear regarding the existence of a fault in the bedrock, approximately 10 m of undisturbed sediment overlie the bedrock. The fault UH-4 at the left side of the figure also does not disrupt the overlying sediment and trends northwest away from the San Simeon fault trend (Plate 6).

Figure 4.5-2 is 4 km north of the Half Graben fault. The projection of the Half Graben fault would cross this line at approximately shot point 900. Locally, the bedrock surface appears to be offset along a trend that connects the southern San Simeon fault zone with the north end of the Half Graben fault zone, and the overlying reflections are either locally draped over a bedrock hump (Figure 4.5-2) or deformed from fault motion; the upper stratigraphy, however, appears undeformed, and no seafloor expression of a fault is present. Along the remainder of the line, evidence for bedrock offset and deformation of the overlying sediment and seafloor is lacking.

Further north (Figures 4.5-3 and 4.5-4), evidence for bedrock offset and deformed overlying stratigraphy is completely lacking. Both of these USGS seismic-reflection profiles north of the Half Graben fault and south of the mapped terminus of the San

Simeon fault exhibit an uninterrupted bedrock unconformity, overlying surficial sediment layers, and an undeformed seafloor.

In the Cambria gap area that is north of the Half Graben mapped fault strands and south of the mapped San Simeon fault strands, a string of relatively high-amplitude magnetic anomalies continues northward along the San Simeon fault zone toward San Simeon Point (Plate 2). Outcrops on the southwestern side of San Simeon Point have been identified as probable Monterey Formation “type” lithology, whereas rocks on the southeastern side of the fault zone are probable Franciscan Complex lithology. Seafloor outcrops 2 to 3 km southwest of San Simeon Point yielded samples dated as belonging to the Luisian and possibly Relizian benthic foraminiferal zones of middle Miocene age (Willingham et al., 2013, Plate 2, their Tables 4 and 5). The onshore part of the San Simeon fault zone cuts through Franciscan Complex rocks with a sliver of ultramafic rocks along the fault zone. The Franciscan Complex rocks are covered by a layer of Quaternary sediment in a shallow bay where the fault zone trends offshore. The magnetic anomalies suggest that the ultramafic rocks continue southeast offshore possibly as far as the north end of the Half Graben fault.

The San Simeon fault zone is interpreted to extend for 8 to 9 km southeast from San Simeon Point (Plate 6). It is composed of three fault segments, the most westerly one being the longest and most continuous. These fault segments are clearly illustrated in the USGS seismic-reflection profiles (Figures 4.5-5 and 4.5-6), with the most westerly fault strand exhibiting vertical separation of an unconformable surface separating the underlying bedrock from a thin (~16 m) cover of surficial sediment and downdropped on the west. The other two segments cut up to the unconformable surface but do not offset it (Figure 4.5-6). The fault strands are acoustically characterized by bent and truncated, fairly continuous, rhythmically layered reflections within the bedrock, and the bounding fault strands separate an internal block of rhythmically layered, westward-dipping reflections in fault contact with chaotic acoustic reflections east and west of the fault block (Figure 4.5-5).

The most easterly strand of the San Simeon fault zone is the next longest segment, being over 5.5 km long. This fault strand bounds the western edge of the nearshore seafloor bedrock exposures and is online with the onshore trend of the San Simeon fault (Plate 6). The other fault strand is short (~4 km long) and is located between the eastern and western segments.

Based solely upon the interpretation of the seismic-reflection profile data available and used in this study, it is not possible to extend the shallow subsurface trace of the San Simeon fault zone further south than its southern terminus as shown on Plates 2 and 6. It is also not possible to extend the near-surface trace of the Half Graben fault further north than is shown on the plates.

A throughgoing bedrock fault that connects the north end of the Half Graben fault zone with the San Simeon fault zone cannot be precluded in the 7 km long zone we have named the Cambria gap. Leslie (1981) and Johnson and Watt (2012) used magnetic data to suggest such a possibility. These data are included in this report as an overlay on Plate 2. As shown above, evidence for recent displacement of the overlying sediment and

seafloor is lacking. There are also no earthquake epicenter locations plotted in this gap area (Plate 6). If there is a throughgoing bedrock fault, then there are three possible reasons it is not observed in the seismic-reflection data:

1. No recent (late Holocene) movement along the fault has taken place and recent slip is taken up on the western strand of the HFZ due west of the gap.
2. Movement along the fault may have taken place in a pure strike-slip motion where flat-lying reflections are not displaced, or that the constant movement of the thin sediment cover masks any deformation produced by the fault.
3. The sediment is very young and is accumulating fairly rapidly from sediment supplied by Santa Rosa Creek and other creeks around San Simeon and swept through the narrow seafloor channels defined by bedrock highs.

#### **4.6 Unassigned Fault Zones**

We use the term “unassigned fault” for those interpreted faults that were not assigned a specific name in the Kingdom program. They are purple (orchid) on the maps and seismic-reflection profiles. In general, the unassigned faults either are separated from the major faults or have a significantly different trend. They may be active (solid line) or buried (dashed line), but they are significantly shorter than the four major fault zones described above (Hosgri, Los Osos, Half Graben, and San Simeon).

Two groups of unassigned faults have been numbered and are discussed in this report. On Plate 6, faults labeled UH-1 to UH-6 are north of the HFZ but on the same trend. They lie in the transition zone between the HFZ and the Piedras Blancas fault and fold belt. These faults are discussed and illustrated in Section 4.2.

To the south of the Los Osos fault zone is a series of parallel northwest-trending faults and folds expressed in bedrock exposures on the inner continental shelf offshore of the west end of the Irish Hills (Plate 4). These faults have been mapped from the USGS 2008 and 2009 LESS data and from the MBES data. This fault zone parallels the Los Osos fault zone, but trends ashore south of where the Los Osos fault zone has been mapped on land (Plate 6). The zone of unassigned faults (U-1 to U-6) trends toward the more rugged and higher-relief area of the Irish Hills. Figure 4.6-1 shows the series of three unassigned faults in this area, along with two anticlinal folds. Further offshore, the faults of this zone control bedrock relief on the seafloor, as exhibited by the fault-parallel ridges that trend into, or are truncated by, the HFZ. These faults have been previously included, in part, in the Los Osos fault zone in previous studies (PG&E 1988, 1990; Johnson and Watt, 2012). The southern faults in this area were named “crowbar” faults on maps, based on interpretation of high-resolution seismic data (PG&E, 1988). However, because the onshore Crowbar Canyon is to the south of Point Buchon, “crowbar” has not been used on later PG&E maps or publications. Due to the extensive bedrock outcrops on the seafloor (Plate 4), this area has limited subsea penetration of the seismic-reflection data. Scattered earthquake epicenters are plotted in the general area of these faults, but direct connections to individual mapped faults are lacking.

Three short unassigned faults and a small swarm of earthquake epicenters are mapped northwest of Morro Bay (Plate 4). The fault segments are online with the offshore extension of the Cambria fault. However, this is an area of limited seismic-reflection data quality (Plate 3), and the fault trends cannot be mapped further toward shore. Localized magnetic anomalies in this area (Plate 2) indicate possible zones of ultramafic rocks similar to those mapped onshore east of Point Estero and Estero Bay.

Plate 4 shows an area of scattered earthquake epicenters in the north-central part of the map. This is an area of very limited data quality (Plate 3), and specific faults and structural trends have not been identified.

## 5.0 COMPARISON WITH PREVIOUS INTERPRETATIONS

This section compares the interpretations undertaken for this study with previous interpretations made using the same data sets as used here. These data sets consist of maps, reports, MBES bathymetry, and various seismic-reflection profile data, as described above.

### 5.1 The 1988 and 1990 LTSP Maps

The PG&E 1988 and 1990 reports to the Nuclear Regulatory Commission (NRC) are docketed items and were widely distributed at that time to PG&E employees, its consultants, technical review boards (USGS and NRC), and organizations requesting copies. The reports are in the public domain. Several editions of structural trend maps were produced at different scales for these reports. The LTSP maps were based on the interpretation of common-depth-point (CDP) multichannel seismic-reflection data collected for resource exploration purposes. The map was produced on three sheets at 1:100,000 scale and on nine sheets at 1:24,000 scale. The three-sheet set was provided with the 1988 report; the nine-sheet set in 1990 was produced in response to a request by NRC reviewers. Another set of maps showing structural trends was titled “Near Surface Faults, Thickness of Post-Late Wisconsinan Sediments and Seafloor Geomorphic Features of the Eastern Offshore Santa Maria Basin.” This latter set was based on interpretation of analog data including profiles from high-resolution seismic-reflection systems (sparkers and boomers), echosounders, and side-scan sonar systems. This map set covered the nearshore area on nine sheets at 1:24,000 scale and showed features that could not be resolved on the deeper CDP data.

This report presents an interpretation that is, in part, a combination of the two map sets described above. It exhibits images of both the shallow features and the majority of the identifiable features at depth. It is based on digitally recorded data from higher-resolution (seismic-reflection profiling and MBES) systems and computer-assisted-analysis and mapping programs.

The data resolution and quality of the maps for the current PG&E study compare to the 1988 and 1990 maps as follows:

- The resolution of seafloor features from the MBES systems far exceeds what could be discerned from the 1980 analog echosounder and side-scan sonar mosaics.
- The quality and resolution of the 2008 and later digitally recorded seismic-reflection data are much better than the analog boomer and mini-sparker records from the 1970s and 1980s.
- The continuity of individual structural trends mapped from high-resolution reflection data integrated with the MBES data is more precise. Even though the features mapped and presented in the 1988 and 1990 PG&E reports may be the same as those in this study, the line-to-line correlations from this study are of better quality.

- The near-surface internal complexity of the fault zones and associated structures is better documented with the post-2008 seismic-reflection profile data.
- Assessments of possible evidence for recency of activity related to seafloor expression or depth of burial are of higher resolution in this study.

The major interpretational differences between this report and the 1988 and 1990 PG&E reports are related to the association of the HFZ and San Simeon fault zone, as follows:

- We found no evidence in the 2008–2009 USGS seismic-reflection profile data or the MBES data sets for extending the San Simeon fault zone along the straight coastline from San Simeon Point to Point Estero or beyond, as was proposed in the 1988 PG&E report.
- The continuity between normal fault segments, and their association with the HFZ, is established in this report, whereas they were mapped as separate segments in the 1988 and 1990 PG&E reports.

We note that this study was limited to data between Point Buchon (Estero Bay) and San Simeon Point, and therefore the comparison between this study and the earlier PG&E studies (PG&E, 1988, 1990) is limited to this area. Not all areas covered by the earlier PG&E studies have been resurveyed since 1988.

## **5.2 Willingham et al. (2013) Paper**

The Willingham et al. (2013) paper was an outgrowth of the PG&E (1988, 1990) studies. It was based on exploration-type high-energy seismic-reflection data, regional bathymetric mapping, and ties with petroleum exploration wells and bottom samples from cores and divers. The paper covered the characterization of the HFZ and associated structures from its southern termination near Point Pedernales to the northern termination north of Point Estero. Three unconformities were mapped and dated in that paper: acoustic pre-Miocene basement, top of Miocene, and the early to late Pliocene. For the most part, these unconformities are beneath the imaging depth of the 2008–2009 USGS data, and the horizon correlations cannot be further delineated in this study area. The post-1988 MBES surveys and the USGS 2008–2009 data were not incorporated into the Willingham et al. (2013) analysis as the latter surveys covered only a small part of the offshore Santa Maria Basin included in that analysis. Also, although the Willingham et al. paper was submitted for publication earlier than Johnson and Watt (2012), delays in reviews and publication prevented direct comparisons between the interpretations of those two sets of authors and this study's interpretations.

Mapping of structural trends in this paper using the MBES, USGS 2008–2009, and Fugro 2010–2011 data undoubtedly improved the location and continuity of the HFZ strands and their near-surface expression (or lack of it) in comparison to the Willingham et al. (2013) maps. However, the 9 km offshore southeast extension of the San Simeon fault zone and the 11 km long Half Graben fault zone and its association with the HFZ are shown on Plate 4 (the structural trend map) of Willingham et al. (2013).

### **5.3 Johnson and Watt (2012) Paper**

Johnson and Watt (2012) undertook an extensive interpretation of the USGS seismic-reflection profile data collected in 2009 and 2010, multibeam (MBES) bathymetry, and magnetic data and produced a detailed structure map with faults located in a manner similar to the one reported here. The main differences between Johnson and Watt's (2012) interpretation and our interpretation lie in the continuation of the San Simeon fault zone south from San Simeon Point to the north end of the Half Graben fault zone, and then further to connect with the HFZ. Johnson and Watt (2012) appear to use the magnetic data as evidence for a continuous connection between the San Simeon fault zone and the HFZ (Figure 13B of Johnson and Watt, 2012). In contrast, in our investigation to examine recent activity of faulting in the area, we did not find evidence for a continuous San Simeon–Hosgri connection in the shallow subsurface or in the USGS seismic-reflection data used in both studies (see Figures 4.5-3 through 4.5-6). Rather, we interpret the most recent movement along the faults in this area as being concentrated along the more westerly trending HFZ, as indicated by offset surficial sediment and seafloor expressions (Figures 4.1-1 and 4.1-4; Plates 2 and 4). Therefore, although we do not preclude the existence of a deep-seated fault in the bedrock that connects the San Simeon fault zone with the Half Graben fault zone, we do not see evidence for recent faulting along the 7 km distance between the two fault zones.

Another difference, if minor, is that Johnson and Watt (2012) include the faults that we have mapped as the “unassigned faults” (see Section 4.6) as part of the Los Osos fault zone. These faults, as mapped by us, trend southeast into the shallow bedrock area offshore of the Irish Hills. Previously, the Los Osos fault zone has been considered the northern bounding fault to the uplifted block of the Irish Hills and the Pismo syncline (PG&E, 1988; Lettis et al., 2004). These faults appear too far south to be part of the bounding structure and possibly are more in line with projections of the (inactive?) Edna fault zone. The results of the recent onshore seismic-reflection survey in the Irish Hills and across the Los Osos fault zone may provide further evidence as to the association and possible recency of activity of this group of faults.

### **5.4 PG&E (2013a) Report**

PG&E (2013a) used the same data sets that were used in this study and in Johnson and Watt (2012) to develop a stratigraphic framework for the assessment of fault activity offshore of Central California between San Simeon Point and Point Sal. The pattern of faulting that PG&E (2013a) shows is similar to ours and that of Johnson and Watt's (2012), except that the PG&E report (2013a) shows faults specifically based on offsets of stratigraphic horizons, and it connects the San Simeon fault zone with the HFZ through a buried inferred fault (see Figures 7-2 and 7-3 and Plate 1 of PG&E, 2013a). The basis for PG&E's (2013a) interpretation of the San Simeon–Hosgri connection is the remarkable straight-line trend of both fault zones that can be interpreted to connect to each other.



## 6.0 CONCLUSIONS

This study was undertaken to better understand the pattern of faulting along the continental shelf between San Simeon Point and southern Estero Bay. It includes an integrated interpretation of all available seismic-reflection and MBES data from that area that are in PG&E's possession. The following data sets are referenced in this interpretation:

- The 1986 COMAP Alaska CDP survey for PG&E.
- The 1974–1982 LTSP deep-penetration seismic-reflection data collected by Western Geophysical and included in PG&E's legacy data archive.
- The 2008 and 2009 USGS LESS and magnetometer data.
- The 2011 Fugro 2D LESS survey for PG&E's Shoreline fault study.
- MBES bathymetric data collected for PG&E in 2007, 2009, and 2010 by the CSUMB Seafloor Mapping Lab.
- 2012 MBES data collected by the USGS.
- Composite DEM, Version 7, from the DCP.P Geodatabase.

Except for the Western Geophysical 1974 to 1982 deep exploration lines, all the data are shown on Plates 2, 4, 5, and 6 as either geophysical survey lines, MBES images of the seafloor and the DEM of the coastal areas.

This study also includes reviews of previous interpretations for the area using the same data sets to compare previously mapped structural patterns with our resulting interpretation and mapping. Included in the reviews are the 1988 and 1990 PG&E LTSP mapping, a paper by Willingham et al. (2013) that used the LTSP data tied into exploration wells, the Johnson and Watt (2012) analysis of the USGS 2008–2009 LESS data, and the recent report by PG&E (2013a) on stratigraphic interpretations of this area.

The MBES data and post-2008 seismic data provide higher-resolution images of both the seafloor morphology and the shallow sub-seafloor sediment and deformed Neogene sedimentary rock horizons than were available for the PG&E LTSP studies (PG&E 1988, 1990) or the Willingham et al. (2013) paper. However, the 2008–2011 LESS data are limited in terms of depth of acoustic penetration and, in many areas, provide little information beneath the surficial (Holocene) sediment layer (Plate 3). As a result, the LESS data allow for alternate interpretations of structural continuity of fault strands and associated folding. For hazards analysis, it is important to understand the relations between the “thin-skinned” deformation observed in the LESS data and the geologic structures that extend to seismogenic depths. Direct shallow to deep correlations have proved difficult because of resolution and accuracy limitations of specific fault strand locations and correlations mapped from the 1970s and 1980s CDP high-energy exploration surveys.

Generally, the pattern of faulting we show is similar to all previous investigations, with the exception of the well-defined or inferred fault connection between the San Simeon fault zone and the HFZ. Johnson and Watt (2012) map this connection as well defined, while Dickinson et al. (2005) infer a connection from previous interpretations, and PG&E (2013a) infers the connection as a buried fault. Johnson and Watt (2012) appear to base

this connection on a linear trend within the magnetic anomaly data. However, we were unable to observe any clear evidence in the seismic-reflection data for a recent fault connecting the San Simeon fault zone with the HFZ (Figures 4.5-3 through 4.5-6). Our interpretations do not preclude the existence of a fault at depth or the possibility of a future rupture along this fault at depth, including propagation to the surface.

From our interpretations, we conclude that the active strands of the HFZ trend more westerly than the general north-south orientation of the San Simeon fault zone, and they control the shelf break in the region (Plate 2). Here the HFZ bounds the inshore (eastern) margin of the offshore Santa Maria Basin as originally mapped by Hoskins and Griffiths (1971). Based on the seafloor expression and offset surficial sediment by the various Hosgri fault strands, we interpret the fault to be active in this area (Figures 4.1-1, 4.1-2, and 4.1-4). The existence of bright spots within reflectors that abut the HFZ indicates that gas has migrated upward from the hydrocarbon generation at depth and is trapped either along the fault or within structures associated with movement along the fault (Figures 4.1-7, 4.2-2, and 4.2-3). Carbonate-like mounds, ridges, and slabs on the outer shelf indicate past fluid seepage onto the seafloor of the upper slope, as shown by depressions on the shelf and lobes of mobilized sediment on the upper slope (Figures 4.1-7, 4.2-2, and 4.2-3; Plates 2 and 4). Thus, the HFZ in this area appears to act as a conduit of fluids migrating from depth that seep out at the surface near the shelf break and destabilize upper-slope sediment.

In the area of the releasing bend of the HFZ described by Johnson and Watt (2012), we map the newly named Half Graben fault zone, a series of faults along which a half graben has formed, downdropped on the east and tilted to the west (Figures 4.4-1 through 4.4-5). This half graben is filled with Quaternary sediment above an erosional bedrock surface (Figure 4.4-3). The half graben is narrow in the north, where it pinches out between bedrock exposed on the inner shelf and a bedrock high exposed along the western side of the graben-bounding fault (Figure 4.4-6; Plate 5). To the south, the half graben widens considerably and appears to end near where the Los Osos fault zone merges with the Half Graben fault zone (Figures 4.4-1 and 4.4-2; Plates 2, 5, and 7). We conclude that the graben originally opened in the south and is presently propagating to the north.

The possibility exists that some Quaternary slip along the HFZ south and west of the Cambria gap has been transferred onto the faults of the transitional zone and over to the Piedras Blancas fold and fault belt. This slip is therefore absorbed within the Piedras Blancas fault and fold belt. With the exception of faults along the south end of the San Simeon fault zone, no good evidence of recent fault displacement is found in this area (Plate 6) offshore inboard (east) of the HFZ.

This study and those of others (PG&E, 2013a; Willingham et al., 2013; Johnson and Watt, 2012) show a series of faults extending northwest from the area adjacent to the onshore Irish Hills. They are south and west of our mapped traces of the Los Osos fault zone. We have labeled these faults as “unassigned” because they appear to be somewhat south of the onshore projections of the Los Osos fault zone. Johnson and Watt (2012), however, have included some of these faults as part of the Los Osos fault zone. Since these faults appear to be associated with seafloor deformation, their possible association

with onshore faulting should be investigated. Once that study is completed, we recommend that those faults be compared to the faults recently mapped by the PG&E onshore vibroseis survey.

## 7.0 LIMITATIONS

Attachment 7.3 of the PG&E Geosciences' Department Procedure CF3.GE2, Quality Related Technical Reports, states: "Address any limitations on the use of results and conclusions" of such report. Therefore, in this section we address limitations of the results and conclusions made herein that may be used within other Geosciences reports.

Because the intent of, and the data used for this report is restricted to the shallow subsurface, the use of the results and conclusions presented in this report to characterize structure at depth, especially within the seismogenic zone is limited. Faults mapped in this study were not correlated with faults and microseismicity at depth, as the 3D seismic-reflection acoustics did not penetrate to depths that would have allowed for such a correlation.

Age estimates are based on the most recent global sea-level curves because biostratigraphic, radiometric, or radiocarbon ages were not available, and age uncertainties of applicable sea-level curves were considered in the dating of horizons and structures.

## **8.0 IMPACT EVALUATION**

Attachment 7.3 to the PG&E Geosciences' Department Procedure CF3.GE2, Quality Related Technical Reports states: "Provide an evaluation of the impact that the results/conclusions have on other Geosciences documents." For this report the impact to other Geosciences documents is unknown at this time.

## 9.0 REFERENCES

- Brown, K.M., 1990. The nature and hydrologic significance of mud diapirs and diatremes for accretionary systems, *Journal of Geophysical Research* **95**: 8969–8982.
- Buchanan-Banks, J.M., Pampeyan, E.H., Wagner, H.C., and McCulloch, D.S., 1978. Preliminary Map Showing Recency of Faulting in Coastal South-Central California, U.S. Geological Survey, Miscellaneous Field Studies, Map MF-910, 3 sheets, scale 1:250,000.
- Dickinson, W.R., Ducea, M., Rosenberg, L.I., Greene, H.G., Graham, S.A., Clark, J.C., Weber, G.E., Kidder, S., Ernst, W.G., and Brabb, E.E., 2005. *Net Dextral Slip, Neogene San Gregorio-Hosgri Fault Zone, Coastal California, Geologic Evidence and Tectonic Implications*, Geological Society of America Special Paper 391, 43 pp.
- DiSilvestro, L.A., Hanson, K.L., Lettis, W.R., and Shiller, G.I., 1990. The San Simeon/Hosgri pull-apart basin, south-central coastal California, *EOS Transactions of the American Geophysical Union* **71** (43): 1632.
- Eichhubl, P., and Boles, J.R., 2000a. Focused fluid flow along faults in the Monterey Formation, coastal California, *Geological Society of America Bulletin* **112**: 1667–1679.
- Eichhubl, P., and Boles, J.R., 2000b. Rates of fluid flow in fault systems—Evidence of episodic fluid flow in the Monterey Formation, coastal California, *American Journal of Science* **300**: 571–600.
- Eichhubl, P., Greene, H.G., and Maher, N., 2002. Physiography of an active transpressive margin basin: High-resolution bathymetry of the Santa Barbara Basin, southern California Continental Borderland, *Marine Geology* **181**: 95–120.
- Eichhubl, P., Greene, H.G., Naehr, T., and Maher, N., 2000. Structural control of fluid flow: Offshore fluid seepage in the Santa Barbara Basin, California, *Journal of Geochemical Exploration* **69-70**: 545–549.
- Fugro Consultants, Inc. (FCL), 2012a. *Field Operations Report 2010-2011 High-Resolution Marine Survey Offshore Diablo Canyon Power Plant, Central California*, prepared for PG&E, May, Fugro Project No. 04.B0992017, 875 pp.
- Fugro Consultants, Inc. (FCL), 2012b. *2D Seismic Data Processing Report 2010-2011 High-Resolution Marine Survey Offshore Diablo Canyon Power Plant, Central California*, prepared for PG&E, May, Fugro Project No. 04.B0992017, 13 pp.
- Fugro Seismic Imaging, 2012. *Seismic Data Processing Report, 3D High-Resolution Marine Survey, California Offshore 2011, Diablo Canyon*, prepared for PG&E, May, Rept. No. 2010-4410\_Draft01, 36 pp.
- Graham, S.A., and Dickinson, W.R., 1978. Evidence for 115 kilometers of right slip on the San Gregorio-Hosgri Fault trend, *Science* **199**: 179–181.

Greene, H.G., and Kennedy, M.P., 1989. Geology of the South-Central California Continental Margin, California Division of Mines and Geology, Continental Margin Geologic Map Series Area 4 of 7, 4 sheets, scale 1:250,000.

Greene, H.G., Maher, N., Naehr, T.H., and Orange, D.L., 1999. Fluid flow in the offshore Monterey Bay region: in Garrison, R.E., Aiello, I.W., and Moore, J.C. (editors), *Late Cenozoic Fluid Seeps and Tectonics Along the San Gregorio Fault Zone in Monterey Bay Region, California*, Pacific Section of American Association of Petroleum Geologists, Volume and Guidebook GB-76, pp. 1–19.

Greene, H.G., Maher, N.M., and Paull, C.K., 2002. Physiography of the Monterey Bay National Marine Sanctuary and implications about continental margin development, *Marine Geology* **181**: 55–82.

Hall, C.A., Jr., 1975. San Simeon–Hosgri Fault System, coastal California: Economic and environmental implications, *Science* **190**: 1291–1294.

Hamilton, D.H., and Willingham, C.R., 1977. Hosgri Fault Zone: Structure, amount of displacement, and relationship to structures of the western Transverse Ranges, *Geological Society of America Abstracts with Programs* **9**: 429.

Hanson, K.L., Lettis, W.R., McLaren, M.K., Savage, W.U., and Hall, N.T., 2004. Style and Rate of Quaternary Deformation of the Hosgri Fault Zone, Offshore South-Central California: in Keller, M.A. (editor), *Evolution of Sedimentary Basins/Onshore Oil and Gas Investigations—Santa Maria Province*, U.S. Geological Survey Bulletin 1995-BB, 33 pp.

Hardebeck, J., 2014. Central California earthquake epicenter locations. Unpublished data provided to PG&E from U.S. Geological Survey earthquake database.

Hartwell, S.R., Finlayson, D.P., Dartnell, P., and Johnson, S.Y., 2013. *Bathymetry and Acoustic Backscatter—Estero Bay, California*, U.S. Geological Survey Open-File Report 2013-1225.

Hoskins, E.G., and Griffiths, R.R., 1971. Hydrocarbon potential of northern and central California offshore: in Cram, I.H. (editor), *Future Petroleum Provinces of the United States—Their Geology and Potential*, American Association of Petroleum Geologists Memoir 15, pp. 212–228.

Hovland, M., and Judd, A.G., 1988. *Seabed Pockmarks and Seepages*, Graham and Trotman, London, 293 pp.

Jennings, C.W., 1994. Fault Activity Map of California and Adjacent Areas, California Division of Mines and Geology, Geologic Data Map No. 6, 1 sheet, scale 1:750,000.

Johnson, S.Y., and Watt, J.T., 2012. Influence of fault trend, bends, and convergence on shallow structure and geomorphology of the Hosgri strike-slip fault, offshore central California, *Geosphere* **8** (6): 1632–1656.

- Kennedy, M.P., Greene, H.G., and Clarke, S.H., 1987. *Geology of the California Continental Margin*, California Division of Mines and Geology, Bulletin 207, 110 pp.
- Lekkerkerk, H.-J., van der Velden, R., Roders, J., Haycock, T., de Vries, R., Jansen, P., and Beemster, C., 2006. *Handbook of Offshore Surveying, Book Two*, Clarkson Research Services Limited, St Magnus House, London, 194 pp.
- Leslie, R.B., 1981. *Continuity and Tectonic Implications of the San Simeon-Hosgri Fault Zone, Central California*, U.S. Geological Survey Open-File Report 81-430, 59 pp.
- Lettis, W.R., DiSilvestro, L., Hanson, K.L., and Shiller, G.I., 1990. The San Simeon/Hosgri pull-apart basin: Implications for late Quaternary activity on the Hosgri Fault Zone: in Lettis, W.R., Hanson, K.L., Kelson, K.I., and Wesling, J.R. (editors), *Neotectonics of the South-Central Coastal California*, Friends of the Pleistocene, Pacific Cell, 1990 Fall Field Trip Guidebook, pp. 91–138.
- Lettis, W.R., Hanson, K.L., Unruh, J.R., and Savage W.U., 2004. Quaternary tectonic setting of south-central California: in Keller, M.A. (editor), *Evolution of Sedimentary Basins/Onshore Oil and Gas Investigations—Santa Maria Province*, U.S. Geological Survey Bulletin 1995-AA, 22 pp.
- McCulloch, D.S., 1987. Regional geology and hydrocarbon potential of offshore central California: in Scholl, D.W., Grantz, A., and Vedder, J. (editors), *Geology and Resource Potential of the Continental Margin of Western North America and Adjacent Ocean Basins, Beaufort Sea to Baja California*, American Association of Petroleum Geologists, Circum-Pacific Earth Science Series, vol. 6, pp. 353–401.
- McCulloch, D.S., 1989. Evolution of the offshore central California margin: in Winterer, E.L., Hussong, D.M., and Decker, R.W. (editors), *The Eastern Pacific Ocean and Hawaii*, Geological Society of America, Boulder, Colo., The Geology of North America series, vol. N, pp. 439–470.
- Mullins, H.T., and Nagel, D.K., 1990. Evidence of shallow hydrocarbons offshore northern Santa Cruz County, California, *American Association of Petroleum Geologists Bulletin* 66 (8): 1130–1140.
- Nagel, D.K., Mullins, H.T., and Greene, H.G., 1986. Ascension submarine canyon, California—Evidence of a multi-head canyon system along a strike-slip margin, *Marine Geology* 73: 285–310.
- NCS SubSea, Inc., 2011. *Navigation Final Report, Diablo Canyon Power Plant 3D Survey*, Job Number J00344-FR-001-001, DCP.P 3D Geophysical Survey, 18 pp.
- Pacific Gas and Electric Company (PG&E), 1974. *Geology of the Southern Coast Ranges and the Adjoining Offshore Continental Margin of California, with Special Reference to the Geology in the Vicinity of the San Luis Range and Estero Bay: Final Safety Analysis Report for Diablo Canyon Power Plant*, Appendix 2D, U.S. Atomic Energy Commission Docket Nos. 50-275 and 50-323.



Pacific Gas and Electric Company (PG&E), 1988. *Final Report of the Diablo Canyon Long Term Seismic Program*, U.S. Nuclear Regulatory Commission Docket Nos. 50-275 and 50-323.

Pacific Gas and Electric Company (PG&E), 1990. *Response to Nuclear Regulatory Commission Questions GSG-12 and GSG-16 on the Final Report of the Diablo Canyon Long Term Seismic Program*, U.S. Nuclear Regulatory Commission Docket Nos. 50-275 and 50-323.

Pacific Gas and Electric Company (PG&E), 2011a. *Progress Report on the Analysis of the Shoreline Fault Zone, Central Coastal California*, report to the U.S. Nuclear Regulatory Commission, PG&E Letter DCL-10-003, 36 pp.

Pacific Gas and Electric Company (PG&E), 2011b. *Shoreline Fault Zone Report: Report on the Analysis of the Shoreline Fault Zone, Central Coastal California*, report to the U.S. Nuclear Regulatory Commission, January. [www.pge.com/myhome/edusafety/systemworks/dcpp/shorelinereport/](http://www.pge.com/myhome/edusafety/systemworks/dcpp/shorelinereport/).

Pacific Gas and Electric Company (PG&E), 2012. *DCPP 3D/2D Seismic Reflection Investigation of Structures Associated with the Northern Shoreline Seismicity Sublineament of the Point Buchon Region*, PG&E Technical Report GEO.DCPP.TR.12.01.

Pacific Gas and Electric Company (PG&E), 2013a. *Stratigraphic Framework for Assessment of Fault Activity Offshore of the Central California Coast Between Point San Simeon and Point Sal*, PG&E Technical Report GEO.DCPP.TR.13.01, 76 pp.

Pacific Gas and Electric Company (PG&E), 2013b. *DCPP Geodatabase, Composite DEM, Version 7*.

Pratson, L.F., Ryan, W.B.F., Mountain, G.S., and Twitchell, D.C., 1994. Submarine canyon initiation by downslope-eroding sediment flow: Evidence in late Cenozoic strata on the New Jersey continental slope, *Geological Society of America Bulletin* **106**: 395–412.

Silver, E.A., and Normark, W.R. (editors), 1978. *San Gregorio–Hosgri Fault Zone, California*, California Division of Mines and Geology, Special Report 137, 56 pp.

Sliter, R.W., Triezenberg, P.J., Hart, P.E., Watt, J.T., Johnson, S.Y., and Scheirer, D.S., 2009 (revised 2010). *High-Resolution Seismic Reflection and Marine Magnetometer Data Along the Hosgri Fault Zone, Central California*, U.S. Geological Survey Open-File Report 2009-1100.

Wagner, H.C., 1974. *Marine Geology Between Cape San Martin and Point Sal, South-Central California Offshore*, U.S. Geological Survey Open-File Report 74-252, 17 pp.

Willingham, C.R., Rietman, J.D., Heck, R.G., and Lettis, W.R., 2013. Characterization of the Hosgri Fault Zone and adjacent structures in the offshore Santa Maria Basin, south-

central California; in Keller, M.A. (editor), *Evolution of Sedimentary Basins/Onshore Oil and Gas Investigations—Santa Maria Province*, U.S. Geological Survey Bulletin 1995-CC, 105 pp.

Yun, J.W., Orange, D.L., and Field M.E., 1999. Subsurface gas offshore of northern California and its link to submarine geomorphology, *Marine Geology* **154**: 357–368.

## INDEPENDENT VERIFICATION OF REPORT

Attachment 1

## REPORT VERIFICATION SUMMARY

| Item | Parameter   | Yes | No* | N/A* |
|------|---|-----|-----|------|
| 1    | Purpose is clearly stated and the report satisfies the Purpose.   | xxx |     |      |
| 2    | Data to be interpreted and/or analyzed are included or referenced.  | xxx |     |      |
| 3    | Methodology is appropriate and properly applied.  | xxx |     |      |
| 4    | Assumptions are reasonable, adequately described, and based upon sound geotechnical principles and practices.                           | xxx |     |      |
| 5    | Software is identified and properly applied. Validation is referenced or included, and is acceptable. Input files are correct.          | xxx |     |      |
| 6    | Interpretation and/or Analysis is complete, accurate, and leads logically to Results and Conclusions.                                   | xxx |     |      |
| 7    | Results and Conclusions are accurate, acceptable, and reasonable compared to the Data, interpretation and/or analysis, and Assumptions. | xxx |     |      |
| 8    | The Limitation on the use of the Results has been addressed and is accurate and complete.   | xxx |     |      |
| 9    | The Impact Evaluation has been included and is accurate and complete.   | xxx |     |      |
| 10   | References are valid for intended use.  | xxx |     |      |
| 11   | Appendices are complete, accurate, and support text.  |     |     | xxx  |

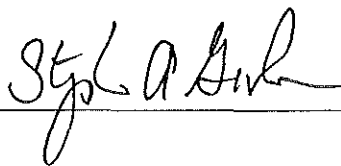
\* Explain "No" or "N/A" entries. (For example, Items 3 thru 7 would be N/A for a data report that simply presents the collected data.)

Comments (use additional pages as necessary):

In my role as ITR for GEO.DCPP.TR.14.05 R0, I met with report co-author Dr. H.Gary Greene to review and discuss interpretations, and subsequently reviewed a draft version of the report in June, 2014. Recommendations from my review were relatively minor, including slight clarifications of language, grammatical errors, and better labeling of figures. Report co-authors Rietman and Greene responded by accepting the recommendations and making requested changes, as verified by me in the final version of the report.

Item 11 of the Verification Summary Report: N/A-- GEO.DCPP.TR.14.05 R0 has no appendices.

Verifier (ITR): Stephan A. Graham  
(name/signature)



3 Sept 2014  
(date)